



## Research paper

## Discovery of a novel, selective CK2 inhibitor class with an unusual basic scaffold



Hend Khalifa<sup>a,1</sup>, Ahmed K. ElHady<sup>a,b,1</sup>, Ting Liu<sup>c</sup>, Walid A.M. Elgaher<sup>d</sup>, Odile Filhol-Cochet<sup>e</sup>, Claude Cochet<sup>e</sup>, Ashraf H. Abadi<sup>a</sup>, Mostafa M. Hamed<sup>d</sup>, Mohammad Abdel-Halim<sup>a,\*\*</sup>, Matthias Engel<sup>c,\*</sup>

<sup>a</sup> Department of Pharmaceutical Chemistry, Faculty of Pharmacy and Biotechnology, German University in Cairo, 11835, Cairo, Egypt

<sup>b</sup> School of Life and Medical Sciences, University of Hertfordshire Hosted By Global Academic Foundation, New Administrative Capital, Cairo, Egypt

<sup>c</sup> Pharmaceutical and Medicinal Chemistry, Saarland University, Campus C2.3, 66123, Saarbrücken, Germany

<sup>d</sup> Helmholtz Institute for Pharmaceutical Research Saarland (HIPS), Helmholtz Centre for Infection Research, Saarland University Campus, 66123, Saarbrücken, Germany

<sup>e</sup> University Grenoble Alpes, INSERM 1292, CEA, UMR Biosante, 38000, Grenoble, France

## ARTICLE INFO

**Keywords:**  
ATP-Competitive inhibition  
Kinase inhibitors  
CK2  
Thienopyrimidines

## ABSTRACT

CK2 is a Ser/Thr-protein kinase playing a crucial role in promoting cell growth and survival, hence it is considered a promising target for anti-cancer drugs. However, many previously reported CK2 inhibitors lack selectivity. In search of novel scaffolds for selective CK2 inhibition, we identified a dihydropyrido-thieno[2,3-d]pyrimidine derivative displaying submicromolar inhibitory activity against CK2 $\alpha$ . This scaffold captured our interest because of the basic secondary amine, a rather unusual motif for CK2 inhibitors. Our optimization strategy comprised the incorporation of a 4-piperazinyl moiety as a linker group and introduction of varying substituents on the pendant phenyl ring. All resulting compounds exhibited potent CK2 $\alpha$  inhibition, with IC<sub>50</sub> values in the nanomolar range. Compound **10b** demonstrated the most balanced activity profile with a cell-free IC<sub>50</sub> value of 36.7 nM and a notable cellular activity with a GI<sub>50</sub> of 7.3  $\mu$ M and 7.5  $\mu$ M against 786-O renal cell carcinoma and U937 lymphoma cells, respectively. **10b** displayed excellent selectivity when screened against a challenging kinase selectivity profiling panel. Moreover, **10b** inhibited CK2 in the cells, albeit less potently than CX-4945, but induced cell death more strongly than CX-4945. Altogether, we have identified a novel CK2 inhibitory scaffold with drug-like physicochemical properties in a favorable basic pKa range.

## 1. Introduction

CK2 is a ubiquitous heterotetrameric Ser/Thr protein kinase belonging to the CMGC group of kinases [1]. CK2 consists of two catalytic  $\alpha$  subunits and two regulatory  $\beta$  subunits [2], however the catalytic subunit of CK2 is believed to be constitutively active [3], and there is evidence that the catalytic CK2 $\alpha$  subunit can also exist as a population independent from CK2 $\beta$  in cells [4]. CK2 is involved in the phosphorylation of hundreds of substrates and controls several signal transduction pathways, therefore its increased activity is associated with several human pathologies [5]. CK2 is an interesting target for cancer therapy as it is involved in the activation of several signal transduction pathways

that enhance cellular proliferation and survival [3,6]. For example, as a co-regulator of anti-apoptotic mechanisms, CK2 phosphorylates BID, preventing its cleavage to the mitochondria-damaging tBID, and the apoptotic mediator caspase 3, causing its inhibition [7].

CK2 overexpression and hyperactivation has been observed in a wide variety of tumors including prostate cancer, breast carcinoma, glioblastoma, leukemias, gastric carcinoma and renal cell carcinoma [8], and targeting CK2 is generally regarded as a promising strategy to achieve tumor regression [9], especially since the first CK2 inhibitor advanced to clinical trials. This compound, CX-4945 (**I**, Fig. 1), also known as silmitasertib, is an ATP-competitive CK2 inhibitor (IC<sub>50</sub> = 14 nM) [10] and currently in phase II clinical trials for the treatment of

\* Corresponding author.

\*\* Corresponding author.

E-mail addresses: [mohammad.abdel-halim@guc.edu.eg](mailto:mohammad.abdel-halim@guc.edu.eg) (M. Abdel-Halim), [ma.engel@mx.uni-saarland.de](mailto:ma.engel@mx.uni-saarland.de) (M. Engel).

<sup>1</sup> authors equally contributed to this work.

cholangiocarcinoma in combination with gemcitabine and cisplatin [11]. Not surprisingly due to the numerous roles of CK2 in human diseases, the clinical studies with silmitasertib were extended to SARS-CoV-2 and influenza virus infections [12]. The phase II study also proved that the inhibition of CK2 in an organism is tolerable despite the numerous effects of CK2 on normal physiological processes, especially since CX-4945 potently inhibits additional kinases, including Clk2 ( $IC_{50} = 4$  nM) [13], Dyrk1A ( $IC_{50} = 6.8$  nM) and Dyrk1B ( $IC_{50} = 6.8$  nM) [14]. In a larger screening against a panel of 238 kinases, further off-targets were detected, such as PIM1, HIPK3 and Clk3, being inhibited with  $IC_{50}$  values in the two-digit nM range [9,15]. These off-target activities could potentially cause severe side effects; e.g., Clk2 inhibition could induce diabetic conditions [16], as Clk2 induces the insulin/Akt pathway causing repression of gluconeogenesis, thus its inhibition would cause hyperglycaemia [17]. Inhibition of Dyrk1A could lead to heart problems, as it is involved in counteracting cardiac hypertrophy through the phosphorylation of NFAT [16]. Altogether, the limited selectivity of CX-4945 might prevent its use for the prolonged treatment of chronic diseases, where CK2 is also implicated in the pathogenic mechanisms, such as neurodegenerative diseases, cystic fibrosis, psychiatric disorders, diabetes, inflammatory and cardiovascular diseases [5]. The more recently developed ATP-competitive CK2 inhibitors were reported to be more selective than CX-4945, for instance the structurally related pyrimidinoquinolines **II** (CX-5011) and **III** (cpd. 2) (Fig. 1) with  $IC_{50}$  values around 3 nM [18–20], as well as the pyrazolopyrimidine **IV** (known as SGC-CK2-1) with an  $IC_{50}$  value of 4.2 nM [21]. Surprisingly, compounds **II** – **IV** proved not very efficient in inducing tumor cell death [20,22]. The most selective cpd. **IV** did not show a significant cytotoxic activity when tested against 176 cancer cell lines at a screening dose of 10  $\mu$ M: only in four of those cell lines, **III** elicited minor lethality (8%–22%), while with most cell lines, only an anti-proliferative effect was observed [21]. Cpd. **IV** (SGC-CK2-1) also inhibited Dyrk2, although with

100-fold lower potency ( $IC_{50} = 440$  nM), while its activity against DRAK1 (STK17A) remained unclear (100% inhibition at 1  $\mu$ M vs.  $IC_{50} > 10$   $\mu$ M) [21]. Lacking an ionizable moiety, **IV** also suffers from poor water solubility [20]. CX-4945 and CX-5011 on the other hand exert a CK2-independent activity in cells, the induction of methuosis, which is characterized by a nonspecific massive internalization of extracellular fluid [23]. Cpd. **V** ( $IC_{20}$  in the original study) was described as a highly potent CK2 inhibitor ( $K_d = 12$  nM) with excellent selectivity; however, its cellular activity was low probably due to poor membrane permeability [24]. The phenolic compounds **VI** ( $IC_{50}$  against CK2: 280 nM) [25] and **VII** (GO289,  $IC_{50}$  against CK2: 7 nM) [26] were both very selective for CK2 but not druglike, as **VI** contains a potential Michael acceptor motif and **VII** a hydrolyzable aldimine substructure, in addition to the potentially labile aryl bromides.

The ATP binding pocket of CK2 displays a strongly positive electrostatic potential around the conserved lysine-68 [27], thus many inhibitors targeting this site are (weakly) acidic compounds (see e.g. Ref. [28], for a recent review). Only a few reported CK2 inhibitors feature basic moieties, for instance **VIII** (14b) [29], in which an aminopropyl side chain was added to the known tetrabromobenzimidazole (TBB) type of ATP-competitive CK2 inhibitors. **VIII** showed moderate activity against CK2 $\alpha$  (23% residual activity in the presence of 5  $\mu$ M **VIII**), indicating that the aminopropyl side chain did not significantly improve the potency of the parent compound TBB ( $IC_{50}$  against CK2 $\alpha$  = 0.15  $\mu$ M) [30]. In addition, PIM-1 and Clk2 were inhibited by **VIII** more strongly than CK2 $\alpha$  [29] in a small panel of typical off-target kinases. Compound **IX** was synthesized as a dual inhibitor of CK2 and BRD4 to potentially overcome drug resistance in cancer therapy [31]. **IX** (44e) showed the most balanced profile with  $IC_{50}$  values against CK2 $\alpha$  and BRD4 of 230 nM and 180 nM, respectively, however, the docking simulations were inconclusive as to whether the basic *N*-methylpiperazine motif rather interacted with CK2 $\alpha$  or BRD4, and how. Finally, a

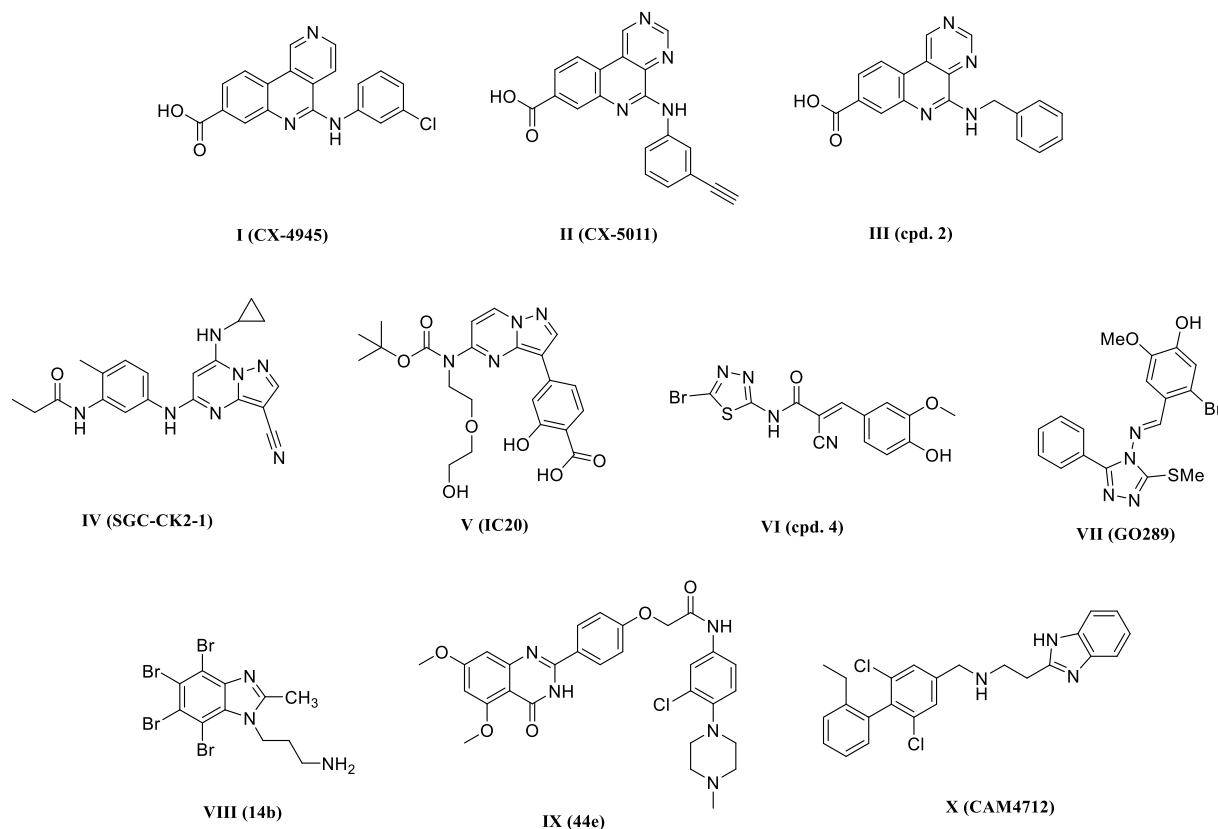


**Fig. 1.** Previously reported CK2 inhibitors. The chart shows potent and selective ATP-competitive inhibitors (I–VII) and miscellaneous dual and allosteric inhibitors with basic moieties (VIII–X).

secondary amine linker was found to be favorable in a group of allosteric CK2 inhibitors, with **X** (CAM4712) being the most potent analogue ( $IC_{50} = 7 \mu M$ ) [32]. The biphenyl portion of **X**, including the secondary amine, bound to the allosteric  $\alpha D$ -pocket, which is relatively distant to the basic center of the ATP binding site (PDB 5OTY). However, despite the allosteric mode of action, **X** significantly inhibited four other kinases: CAMK1, SmMLCK, EF2K and SGK1.

Therefore, there is still a need for developing new chemotypes of CK2 inhibitors with high selectivity and efficacy in cancer cells. Herein we report the discovery of thienopyrimidine derivatives as a novel class of CK2 inhibitors that feature a basic moiety at the core structure.

## 2. Results and discussion

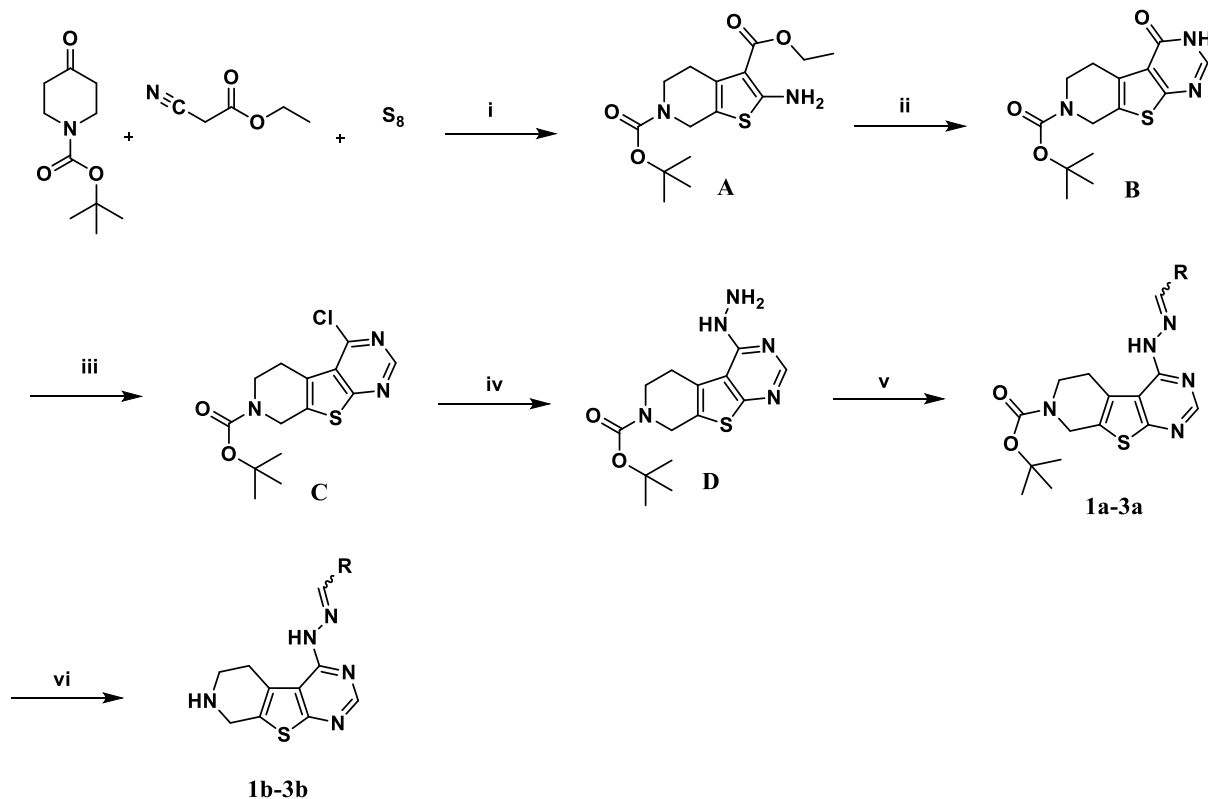
### 2.1. Chemistry

The synthesis of the polysubstituted 2-aminothiophene (intermediate **A**) was achieved through Gewald reaction which is a one-pot procedure of 3 components;  $\alpha$ -methylene carbonyl compound,  $\alpha$ -activated acetonitrile and sulfur. This was followed by the construction of thieno [2,3-*d*]pyrimidine ring system by reacting intermediate **A** with formamidine acetate through modified Niementowski quinazoline reaction to afford intermediate **B** in a good yield. Next, chlorination of

intermediate **B** was achieved in highest yields by using a mixture of  $POCl_3$ :TEA in a ratio 1:3 to give intermediate **C**. Synthesis of intermediate **D** (Scheme 1) was accomplished by  $S_NAr$  reaction of hydrazine hydrate with intermediate **C**. Afterwards, intermediate **C** was reacted with different aldehydes in a nucleophilic addition–elimination reaction to give the hydrazone derivatives **1a-3a**. On the other hand,  $S_NAr$  reaction of intermediate **C** with the appropriate substituted piperazines yielded intermediates **3a-16a** (Scheme 2). Finally, a BOC-deprotection step of intermediates **1a-16a** using trifluoroacetic acid was made to obtain compounds **1b-16b** as TFA salts in good yields.

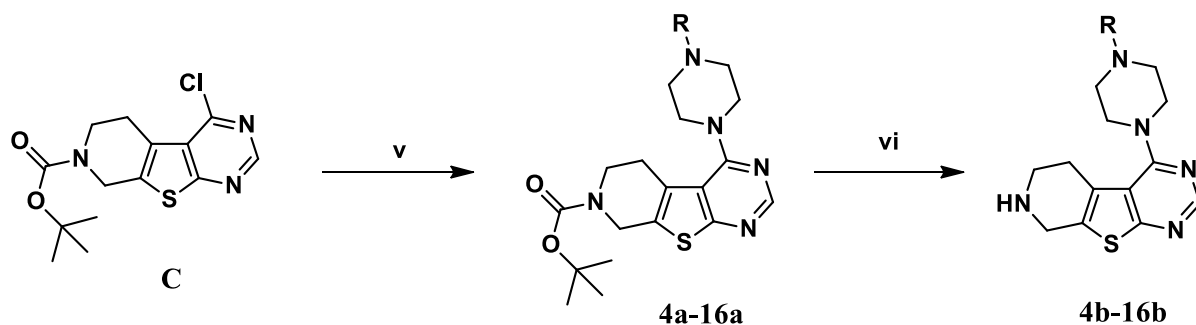
### 2.2. Hit identification and compound design

In an attempt to discover new chemotypes of CK2 inhibitors, we screened an in-house library against protein kinase CK2 $\alpha$  and obtained compound **XI** as an interesting hit (see Fig. 2 for the structure), exhibiting an  $IC_{50}$  value of 143 nM. **XI** contained a cyclic secondary amine, which was rather unusual for a CK2 inhibitor. This prompted us to start optimizing the structure. Our planned strategy (Fig. 2A) included (i) a limited number of other hydrazone derivatives (**1b-3b**), where the synthetic pathway would potentially give access to numerous derivatives by coupling aryl aldehydes to intermediate **D** (Scheme 1). In parallel, we also envisaged to replace the rather unstable hydrazone



Cpd No.	R	Cpd No.	R	Cpd No.	R
1	3-bromophenyl	2	4-bromophenyl	3	1-naphthyl

**Scheme 1.** Synthesis of compounds **1b-3b**. Reagents and conditions: (i) triethylamine, absolute ethanol, rt, 16h; (ii) formamidine acetate, DMF, 100 °C, 4 days; (iii) phosphorous oxychloride, triethylamine, 55 °C, 5h; (iv) hydrazine hydrate, methanol, 70 °C, 3h; (v) aryl aldehyde, ethanol, 80 °C, overnight; (vi) trifluoroacetic acid, DCM, rt, 4h.



Cpd No.	R	Cpd No.	R
4	acetyl	11	2-methylphenyl
5	methylsulfonyl	12	3-methylphenyl
6	phenyl	13	4-methylphenyl
7	2-fluorophenyl	14	2-methoxyphenyl
8	3-fluorophenyl	15	3-methoxyphenyl
9	4-fluorophenyl	16	4-methoxyphenyl
10	4-chlorophenyl		

**Scheme 2.** Synthesis of compounds **4b-16b**. Reagents and conditions: (v) substituted piperazine, ethanol, 80 °C, overnight; (vi) trifluoroacetic acid, DCM, rt, 4 h.

substructure by a more druglike moiety; a superimposition showed that incorporation of piperazine as a linker placed the pendant phenyl ring in a similar position as in the (*E*)-isomer of the corresponding hydrazone (Fig. 2B), suggesting that the piperazine derivative could adopt a similar binding mode. Hence, (ii) a small set of piperazine compounds was also planned, ending with plain phenyl (**6b**) or with small polar groups to probe the binding pocket with H-bond acceptors (**4b**, **5b**).

As detailed in Table 1, compounds **1b-5b** failed to show appreciable CK2 inhibition whereas the phenylpiperazine analogue **6b** ( $IC_{50} = 43$  nM) turned out to be a 3 times more potent inhibitor of CK2 $\alpha$  than the hit compound **XI**. Having thus identified the piperazine moiety as a superior linker, further optimization of the potency was attempted by synthesizing a focused series of **6b** derivatives, where the phenyl ring was substituted with various substituents (compounds **7b-16b**).

### 2.3. Compound optimization

The synthesized series of substituted phenylpiperazines (compounds **7b-16b**) were tested against purified CK2 $\alpha$  at 0.5  $\mu$ M (Table 2). The electron density of the phenyl ring was modulated through its substitution with electron-withdrawing (fluorine and chlorine) and electron-donating groups (methyl and methoxy). Interestingly, all the synthesized compounds were able to achieve CK2 inhibitory potency in the nanomolar range and mostly showed enhanced inhibition in comparison to the hit compound **6b**. The three fluorophenyl regioisomers (compound **7b**: *o*-fluoro, compound **8b**: *m*-fluoro, and compound **9b**: *p*-fluoro) showed a moderate 1.5 to 2-fold increase in CK2 inhibitory potency. Introducing a larger halogen in compound **10b** (*p*-chloro) did not further enhance the activity as it was almost equipotent to compound **6b** with an  $IC_{50}$  of 36.7 nM.

On the other hand, the *m*-methyl substituted compound **12b** was found to be 19-fold and 6-fold more potent than compounds **XI** and **6b**, respectively, attaining a single-digit nanomolar  $IC_{50}$  of 7.5 nM. The remaining compounds in the series with either a methyl or a methoxy

substituent in different positions: *o*-methyl (**11b**), *p*-methyl (**13b**), *o*-methoxy (**14b**), *m*-methoxy (**15b**) and *p*-methoxy (**16b**) inhibited CK2 $\alpha$  with similar  $IC_{50}$  values, ranging from 15.7 nM to 22 nM, thus eliciting a slight 2-fold improvement in potency compared to compound **6b** ( $IC_{50} = 43$  nM). Altogether, the structure-activity relationships pointed to an activity-enhancing function of the terminal methyl group, with a varying strength depending on the position. In agreement with this, our docking simulation with **12b** predicted a CH- $\pi$  interaction of the methyl with Phe113 (Fig. 7).

### 2.4. Inhibition of cell growth by the tetrahydropyrido thieno[2,3-*d*]pyrimidine derivatives

The potency to inhibit cell growth of cancer cells was tested for all compounds using the renal cell carcinoma cell line 786-O. This cell line was chosen because its viability is strongly susceptible to intracellular CK2 inhibition [10]. To our surprise, the most potent derivative in the cell free assay, **12b**, showed only a weak inhibition of cell growth, with a  $GI_{50}$  value around 30  $\mu$ M, the highest tested concentration (Table 2). **8b** and **13b** moderately inhibited cellular growth with  $GI_{50}$  values of 15 and 14.7  $\mu$ M, respectively. Although compound **10b** was not the strongest CK2 inhibitor among the other substituted phenylpiperazine analogs ( $IC_{50} = 36.7$  nM), it showed the highest activity in cells with a  $GI_{50}$  of 7.3  $\mu$ M. On the other hand, the more polar, methoxy-substituted derivatives were among the weakest inhibitors of cell growth. These findings suggest that in addition to the potency against CK2, the compounds might also need sufficient lipophilicity to be cell permeable. Under the same conditions, the reference inhibitor CX-4945 displayed a  $GI_{50}$  of 5.5  $\mu$ M against the 786-O cell line (Tables 2 and 3).

Although compound **XI** exhibited a cell growth inhibition similar to compound **10b** with a  $GI_{50}$  of 6.6  $\mu$ M, its markedly high cytotoxicity compared to the less potent inhibition in the cell-free assay might be attributed to the bromophenyl hydrazone moiety; **XI** might be prone to enzymatic or chemical hydrolysis in cells releasing the toxic

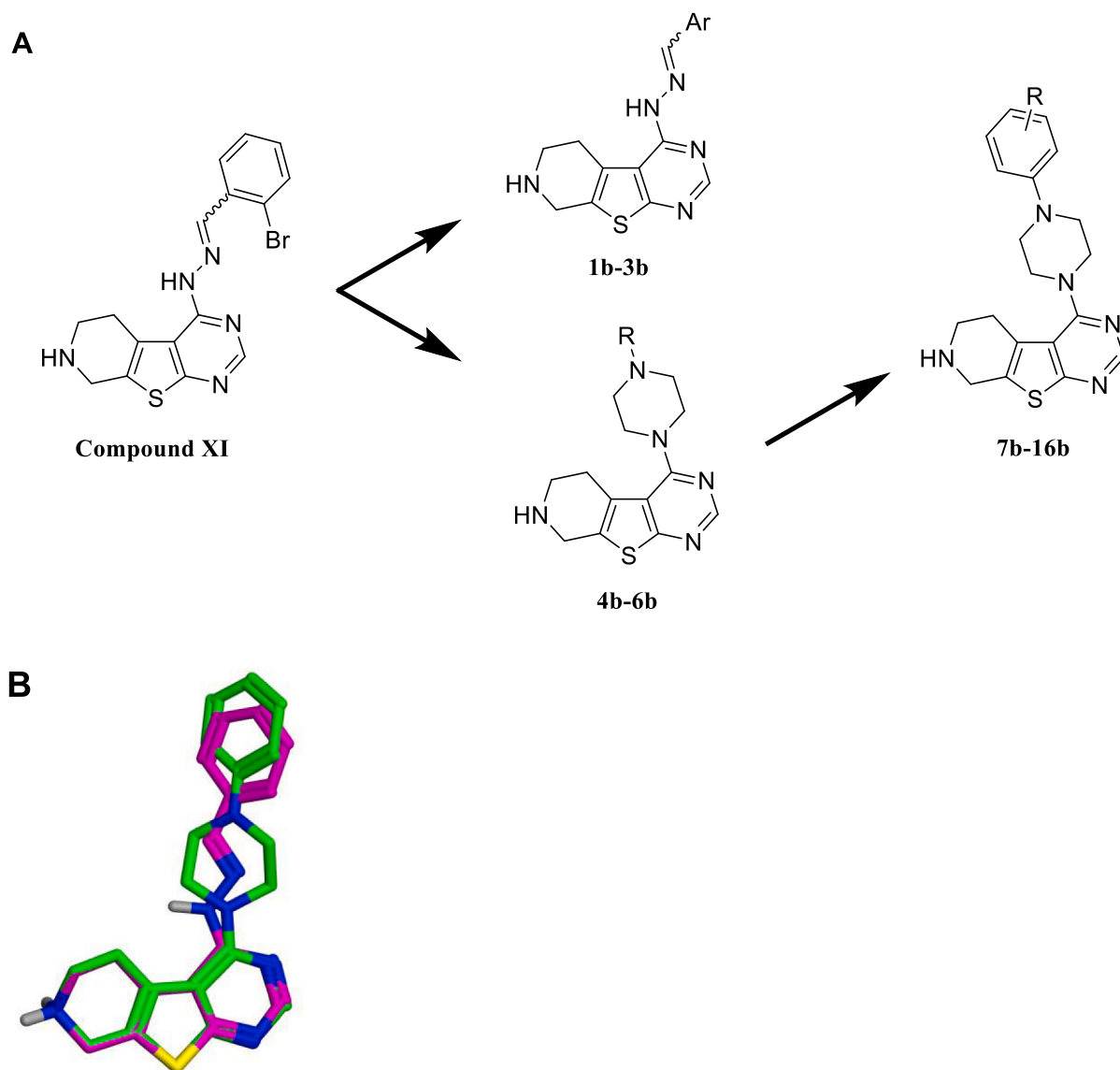


**Fig. 2.** Optimization of hit compound XI. (A) planned compound modifications. (B) Superimposition of an (*E*)-hydrazone (magenta) and a piperazine (green) model compound.

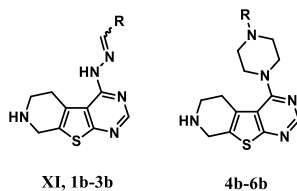
bromobenzaldehyde, which might contribute to a general cytotoxicity [33]. Therefore, compound **10b** with the new, more stable scaffold but not **XI** was selected for further characterization. Further testing of **10b** along with reference inhibitors against the U973 lymphoma cell line revealed a  $GI_{50}$  of 7.5  $\mu$ M, similar that against 786-O cells, whereas the  $GI_{50}$  against the non-tumor cell line HEK293 was 30  $\mu$ M (Table 3), indicating some degree of tumor cell selectivity. Notably, the reference compound SGC-CK2-1 was significantly more potent than **10b** or CX-4945 to inhibit U937 cell growth.

### 2.5. Induction of cell death by **10b**

Inhibition of CK2 in tumor cells is expected to induce cell death [34, 35]. However, a paradox was encountered with some recently developed, potent ATP-competitive CK2 inhibitors: the more selective for CK2, the less potent was the induction of tumor cell death, although cellular target engagement was proven by nanoBRET assays. Poor cytotoxic activity against tumor cell lines was reported for the selective CK2 inhibitors SGC-CK2-1 (**IV** in Fig. 1) [20,22], CX-5011 (**II**) and compound 2 (**III**) [20]. Furthermore, even the less selective CX-4945

exhibited no cytotoxicity against MDA-MB-231 breast cancer and A375 melanoma cells when treated for 48 h with concentrations between 5 and 10  $\mu$ M [20,36]. In 786-O cells, the induction of cell death at 4  $\mu$ M CX-4945 was weak to moderate but somewhat higher than with SGC-CK2-1 [36]. Earlier studies reporting a stronger impact on cell viability by CX-4945 employed MTT or WST-1 assays that may rather have measured the inhibition of cell proliferation [37,38]. The reason for the poor cytotoxic activity despite blocking the ATP binding pocket of CK2 in tumor cells is not clear, but this circumstance indicates that even highly potent ATP-competitive CK2 inhibitors must be checked for their capacity to induce tumor cell death in order to assess their potential for development into effective anti-cancer drugs. Hence, we used the CellCyteX live-cell microscopy system to specifically measure the cell death rate of 786-O cells in the presence of **10b**. As shown in Fig. 3, **10b** concentration-dependently triggered cell death starting approx. 11 h after addition of the compound. CX-4945 did not affect cell viability at the highest concentration applied (5  $\mu$ M) under the same conditions. The poor efficacy of CX-4945 and SGC-CK2-1 to induce cell death in 786-O cells was in agreement with previously published data [36].

**Table 1**  
Inhibition of recombinant CK2 $\alpha$  by the synthesized probe compounds.



Cpd No.	R	CK2 %inhibition @ 0.5 $\mu$ M <sup>a</sup>	IC <sub>50</sub> (nM) <sup>b</sup>	Cpd No.	R	CK2 %inhibition @ 0.5 $\mu$ M <sup>a</sup>	IC <sub>50</sub> (nM) <sup>b</sup>
XI		86.7	143	4b		31.5	n.d.
1b		34.7	n.d.	5b		0	n.d.
2b		40	n.d.	6b		82.7	43
3b		39.1	n.d.				

<sup>a</sup> Mean values of duplicates that differed by no more than 10 %.

<sup>b</sup> Values are the mean of at least two independent experiments, SD  $\leq$  12 %. n.d., not determined.

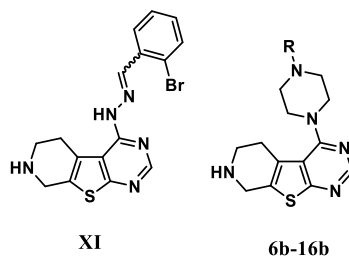
## 2.6. **10b** inhibits CK2 in cells

Next, we analyzed whether the cytotoxic activity of **10b** against the 786-O cells was due to intracellular inhibition of CK2. To this end, the 786-O cells were cultured in the presence of **10b** or DMSO as solvent control for 48h. CX-4945 was also included for comparison. The total cellular proteins were then analyzed by immunoblotting (Fig. 4A and B), first applying an antibody developed to recognize phosphosites generated by CK2, which had previously been validated with lysate from CK2 $\alpha/\alpha^{(-/-)}$  knockout cells [39]. As can be seen in Fig. 4A, treatment of the 786-O cells by **10b** led to reduced signals of almost all CK2 phosphosites in a concentration-dependent manner. A peculiar exception was a band at 95 kDa, which was not present in the DMSO control, however, it appeared even more prominent with the reference inhibitor CX-4945. The six most abundant signals (denoted by arrowheads) were also quantified, revealing that four of these CK2-dependent protein phosphorylations were inhibited stronger by CX-4945 than by our new inhibitor **10b** (Table at the bottom of Fig. 4A). To complement our data, we carried out the same experiment with the non-adherent, hematological cancer cell line U937 (Fig. 4C). Here, the anti-CK2 phosphosite antibody produced only a few prominent signals against the background, similar to previously published results with the same cell line and antibody [40]. A low number of signals had also been detected in U2OS cells using the same antibody [41], suggesting that only the most abundant CK2 substrates may produce a recognizable signal. In our experiment, the two most prominent signals with U937 cell lysates were decreased more potently by CX-4945 and SGC-CK2-1 than by **10b** (Fig. 4C). Interestingly, the more selective inhibitor SGC-CK2-1 (IV in Fig. 1) was less potent than CX-4945 against the phosphorylated protein no. 2, and only about two times more effective than **10b** in reducing the corresponding signal intensity (cf. densitometric analysis at the bottom of Fig. 4C). Considering the rather potent inhibition of U937 cell growth by SGC-CK2-1 (GI<sub>50</sub> = 1.8  $\mu$ M, Table 3), we decided to check for signs of apoptosis induction by re-probing the same Western Blot using an

anti-PARP antibody that recognizes both the cleaved and uncleaved form. As can be seen in Fig. 4C, PARP cleavage occurs in the presence of **10b**, beginning at the 5  $\mu$ M concentration similar to CX-4945, but was weaker with SGC-CK2-1. Altogether, these data suggest that the CK2 substrate phosphorylations inhibited by SGC-CK2-1 in U937 cells are more crucial for cell proliferation than for cell survival.

Next, phospho-specific antibodies were used to analyze CK2-dependent phosphorylations of single substrate proteins in 786-O cells (Fig. 4B). Among them, the eukaryotic translation-initiation factor eIF2 $\beta$  was reported to form a tight complex with protein kinase CK2 [42], and Ser-2 was confirmed to be a *bona fide* CK2 substrate site, the phosphorylation of which could effectively be suppressed by different CK2 inhibitors [43]. Furthermore, STAT3 can be phosphorylated by CK2 in a complex as identified in CML cells [44], but also indirectly through JAK2 following to phosphorylation and activation of the latter kinase by CK2 [45,46]. Finally, we analyzed phospho-cdc37-Ser13 as another CK2-dependent phosphorylation site [47]. After incubation of 786-O cells with **10b** for 48h, the strongest inhibition of phosphorylation was noted for STAT3, almost equally potent to the reference inhibitor CX-4945 (Fig. 4B, densitometric quantification at the bottom). The phospho-eIF2 $\beta$ -Ser2 signal was also markedly reduced after treatment by **10b** for 48 h, whereas only a weak inhibition of the Ser13-phosphorylation at cdc37 was observed; however, CX-4945 also failed to fully suppress cdc37 phosphorylation. While cdc37-Ser13 was originally identified as a target site of CK2 [47], it has been found more recently that some degree of phosphorylation at this site was retained in CK2 $\alpha/\alpha^{(-/-)}$  knockout cells, indicating that Ser13 of the molecular chaperone cdc37 can also be phosphorylated by other protein kinases [39]. Eventually, we also analyzed the cellular amounts of CK2 $\alpha$  and CK2 $\alpha'$  in 786-O cells after treatment with **10b** and found no change (Fig. S2). Overall, our data confirmed that **10b** inhibited CK2 in 786-O cells at concentrations consistent with the observed GI<sub>50</sub> value (Tables 2 and 3). Moreover, the onset of cell death induced by **10b** also occurred between 5 and 10  $\mu$ M (Fig. 3 and Fig. S3). Paradoxically, the

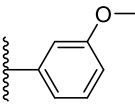
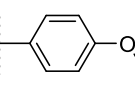
**Table 2**  
Inhibition of recombinant CK2 $\alpha$  and cell growth of 786-O renal cancer cells.



Cpd No.	R	CK2 %inhibition at 0.5 $\mu\text{M}^a$	IC <sub>50</sub> (nM) <sup>b</sup>	786-O renal cell %inhibition at 30 $\mu\text{M}^a$	GI <sub>50</sub> ( $\mu\text{M}$ ) <sup>b</sup>
XI		86.7	143 $\pm$ 13.7	99.2	6.6 $\pm$ 0.2
6b		82.7	43 $\pm$ 2.4	15.9	n.d.
7b		66.7	39.2 $\pm$ 7.4	35.8	n.d.
8b		75.3	29.7 $\pm$ 5.1	74.6	15 $\pm$ 3.2
9b		91.2	20 $\pm$ 4.7	25.3	n.d.
10b		76.2	36.7 $\pm$ 2.9	102	7.3 $\pm$ 0.4
11b		93.4	15.7 $\pm$ 6.8	52.1	30 $\pm$ 1.9
12b		94.8	7.5 $\pm$ 3.1	47.2	n.d.
13b		83.8	17.8 $\pm$ 0.6	78.2	14.7 $\pm$ 1.4
14b		93.4	18.2 $\pm$ 1.0	36.7	n.d.

(continued on next page)

Table 2 (continued)

Cpd No.	R	CK2 %inhibition at 0.5 $\mu\text{M}^a$	IC <sub>50</sub> (nM) <sup>b</sup>	786-O renal cell %inhibition at 30 $\mu\text{M}^a$	GI <sub>50</sub> ( $\mu\text{M}$ ) <sup>b</sup>
15b		95.1	22 $\pm$ 0.1	50.2	29.5 $\pm$ 2.9
16b		81.9	17.4 $\pm$ 4.7	27.7	n.d.
I (CX-4945) <sup>c</sup>		97.7	7.3 $\pm$ 2.4	n.d.	5.5 $\pm$ 1.0

<sup>a</sup> Mean values of duplicates that differed by no more than 10 %.

<sup>b</sup> Data presented are the mean of at least two independent experiments. IC<sub>50</sub> and GI<sub>50</sub> values are given  $\pm$  SD.

<sup>c</sup> See Fig. 1 for structure. n.d., not determined.

Table 3

Cell growth inhibition of non-tumor vs. tumor cell lines.

cpd.	GI <sub>50</sub> value ( $\mu\text{M} \pm$ SD)		
	HEK293 (human embryonal kidney cells)	U937 (histiocytic lymphoma)	786-O (renal cancer cells)
10b	30 $\pm$ 0.5	7.5 $\pm$ 0.8	7.3 $\pm$ 0.4
CX-494	>30	4 $\pm$ 0.3	5.5 $\pm$ 1.0
SGC-CK2-1	>30	1.8 $\pm$ 0.2	5.7 $\pm$ 0.8

reference inhibitors CX-4945 and SGC-CK2-1 did not trigger cell death of 786-O cells at concentrations up to 20  $\mu\text{M}$  (Fig. 3), although both inhibited CK2-dependent phosphorylations in cells more potently than 10b. With respect to SGC-CK2-1, this discrepancy was in agreement with the original findings of Wells and colleagues [21]: the CK2-dependent phosphorylations of AKT1 and eIF2 $\beta$  were inhibited by SGC-CK2-1 in HCT116 cells with IC<sub>50</sub> values below 100 and 500 nM, respectively, whereas the proliferation of the same cell line was not affected (GI<sub>50</sub> value > 10  $\mu\text{M}$ ). However, when SGC-CK2-1 was screened against 140 cancer cell lines using a different protocol, GI<sub>50</sub> values in the single-digit  $\mu\text{M}$  range were found with most cell lines, including HCT-116 cells [21]. Nonetheless, the relatively weak activity against cell lines has given rise to contrasting interpretations [21,48]. Hence, further research is needed to clarify why the high efficacy of SGC-CK2-1 in inhibiting CK2-catalyzed substrate phosphorylation in cells does not translate to an equally potent antiproliferative and especially apoptosis-inducing effect. It was observed that some cellular CK2 phosphosites are more sensitive toward SGC-CK2-1 treatment than others [21,49], thus the apparently poor efficacy of SGC-CK2-1 against tumor cells might just indicate that some CK2-regulated pathways that promote cell survival and proliferation are among those that are not sufficiently blocked. Detecting such “resistant” pathways is complicated by the large number of CK2 substrates, counting several hundred [50], more than 760 according to the PhosphoSitePlus database [49], several of which may contribute to tumor cell survival or proliferation. It should be noted that especially the protection against apoptosis is usually reinforced by many complementary pathways [51,52].

### 2.7. Selectivity profiling of 10b against typical off-target kinases of CK2 inhibitors

Inhibitors targeting the CK2 ATP binding pocket, irrespective of the chemotype, share a common set of notorious off-targets, mainly PIM1, Dyrk2, HIPK2, DAPK3 (ZIPK), PRKD1 (PKC $\mu$ ), FLT3/4 and TBK1 [19,30]. A smaller subset of the typical off-targets is still affected by some of the more selective kinase inhibitors such as CX-4945 (I in Fig. 1), CX-5011 (II) [19], compound 2 (III), IC20 (V) [20] and GO289 (VII) [26]. Based on the previously identified off-targets we composed a challenging panel of kinases against which compound 10b was screened. As shown in Table 4, 10b showed no significant inhibitory

activity against the screened list of kinases at a screening dose of 2  $\mu\text{M}$ , except for the close homologue CK2 $\alpha'$  (CSNK2A2) that was moderately inhibited by 57 %. Thus, it can be concluded that 10b is a highly selective CK2 inhibitor.

### 2.8. Investigation of the binding mode

First, we tested whether the inhibition of CK2 $\alpha$  by 10b was affected by the concentration of ATP. To this end, the inhibition assay was performed with 50 nM 10b, slightly above the IC<sub>50</sub> value. ATP concentrations of 15, 50 and 100  $\mu\text{M}$  were used, giving a percent inhibition of 54 ( $\pm$ 3 %), 58 ( $\pm$ 7 %) and 34 % ( $\pm$ 5 %), respectively. Thus, the CK2 inhibition by 10b was not strictly ATP-competitive, only at higher ATP concentrations. Since a binding of 10b in an allosteric pocket communicating with the ATP binding site could not be ruled out, the activity of compound 10b was then measured against the holoenzyme CK2 $\alpha_2\beta_2$ . As shown in Fig. 5, Compound 10b was able to inhibit both the catalytic subunit CK2 $\alpha$  and the CK2 holoenzyme with comparable potency (IC<sub>50</sub> = 40–50 nM), indicating that the binding site of 10b was not located at the  $\alpha/\beta$  interface site on CK2 $\alpha$ , which harbors a known binding pocket for allosteric ligands [53,54].

To test for binding of 10b in the ATP pocket, a competition assay was performed using surface-plasmon resonance (SPR) analysis. His<sub>6</sub>-tagged CK2 $\alpha$  was non-covalently immobilized on a Ni<sup>2+</sup>-coated sensor chip. After injection of 10b at different concentrations, binding could be detected (Fig. 6) with a calculated  $K_d$  value of 130 nM under these conditions, where 1 % DMSO was included in the sample and running buffer. This amount of DMSO might have affected the hydrophobic interactions by 10b, thus increasing the measured  $K_d$  value [55,56]. CX-4945 was then included in the running buffer at a concentration of 1  $\mu\text{M}$ , so that the ATP binding pocket of the immobilized CK2 $\alpha$  was permanently saturated with this ATP-competitive ligand. When 10b was injected again using the same settings as before, binding to CK2 $\alpha$  was completely abolished. This result indicated that the binding site of 10b was the ATP pocket or at least overlapped with the CX-4945 binding site.

The basic nature of the compounds and the non-linear competition with ATP made an unusual binding mode conceivable, different from binding to the ATP pocket in its common active conformation. Considering the highly flexible nature of several structural elements in CK2 $\alpha$  [57,58], we contemplated that our compounds might bind to a



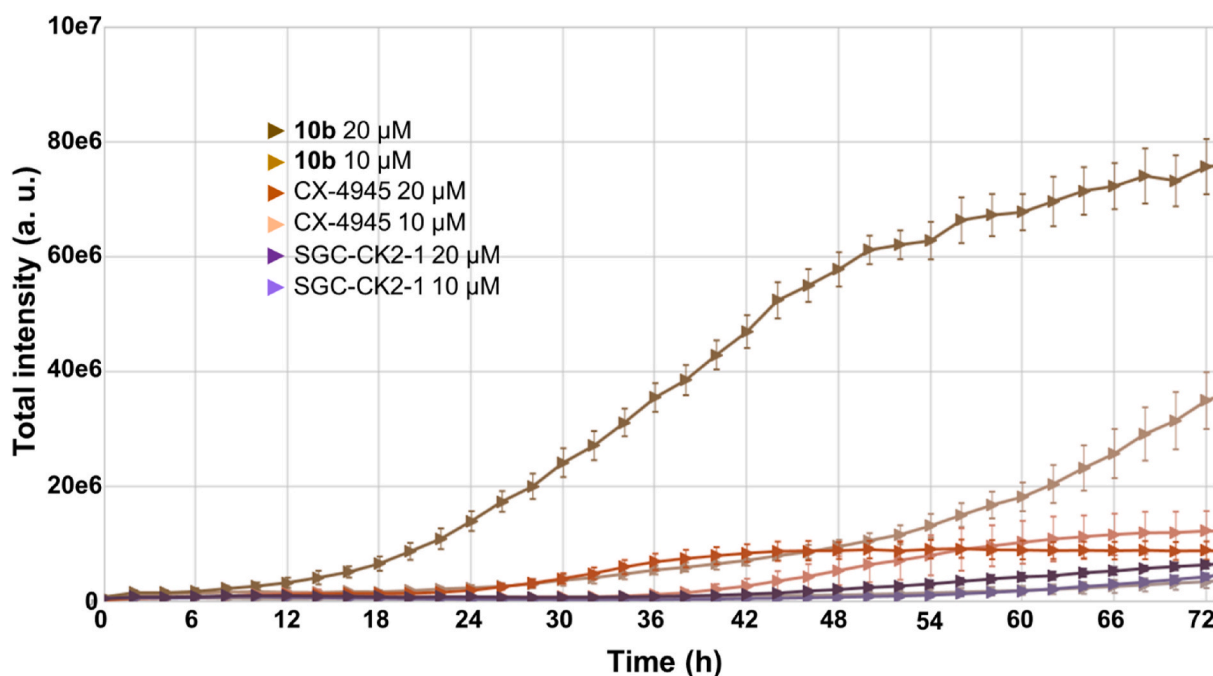


**Fig. 3.** Induction of cell death by **10b**. 786-O cells were treated for indicated time with different concentrations of **10b**, CX4945 or SGC-CK2-1. Cell viability was recorded using Cytotox Green reagent in the CellCyteX live-cell microscope. The experiment shown is representative of three independent measurements.

particular conformation of the ATP pocket, which might have a lower affinity for ATP. An alternative closed conformation, in which the hinge region and the subsequent  $\alpha$ D helix shifted their positions, had been observed in several crystal structures of CK2 $\alpha$ , which were obtained dependent on the pH of the crystallization buffers and/or the presence of stabilizing ligands such as emodin [58,59]. Of note, the particular form of the ATP pocket with closed hinge/ $\alpha$ D conformation has not yet been specifically addressed for ligand development. We used both the active, open conformation – which is the form binding ATP for catalysis – and the closed conformation as templates for docking of our most potent compound, **12b**. In both the predicted binding models (Fig. 7), the orientation of the secondary amine of **12b** toward the hinge binding region (western part of the illustration) avoided electrostatic repulsion by the strongly positive electrostatic potential prevailing around Lys68. While in both models, the eastern part of the interactions with the ligand was mostly similar, involving multiple CH- $\pi$  and hydrophobic interactions around the 3-methylphenyl moiety, the distinct conformations of the flexible hinge region accounted for different binding modes of the tricyclic ring; for the closed hinge/ $\alpha$ D conformation (Fig. 7A), a stronger set of interactions was predicted than for the open conformation (Fig. 7B), also reflected by the docking scores of  $-27.9$  vs.  $-24.6$  kcal/mol, respectively. Moreover, the model could explain the higher potency of **12b** compared with the other congeners (**7b–11b**, **13b–16b**), as the 3-methylphenyl ring was favorably accommodated in the most hydrophobic area of the ATP-binding pocket, with the methyl group engaging in CH- $\pi$  interactions with the gate keeper residue Phe113. Altogether, the closed hinge/ $\alpha$ D conformation appears to be more compatible with binding of **12b** than the open conformation. It should be noted that this would be different from all other potent CK2 inhibitors developed in the last decades that bind to the open hinge form, such as CX-4945 (**I** in Fig. 1) (PDB: 3NGA), CX-5011 (**II**) (PDB: 3PE2) and SGC-CK2-1 (**IV**) (PDB: 6Z83), similarly to AMPPNP, a non-hydrolysable form of ATP (PDB: 8QCG).

### 3. Conclusions

In the present study, we have reported the design, synthesis, and

biological evaluation of a novel class of 4-substituted tricyclic dihydropyrido-thienopyrimidine derivatives as promising CK2 inhibitors. Among the optimized analogs, compound **10b** showed the best balance between cell-free potency ( $IC_{50} = 36.7$  nM) and cell growth inhibition ( $GI_{50} = 7.3$   $\mu$ M). We obtained evidence that the novel compounds were directed towards the ATP binding site, but radiometric ATP competition assays and molecular docking suggested that the partially inactive, closed hinge/ $\alpha$ D conformation was more likely to be recognized by the ligands than the open hinge conformation, which corresponds to the active form that is competent for ATP binding.

Thus, we presented, to the best of our knowledge, the first potent CK2 inhibitor scaffold with a basic moiety at the core structure that addressed the ATP binding pocket. Most of the reported CK2 inhibitors in literature act in an ATP-competitive manner [60]. A basic moiety is frequently found in such kinase inhibitors [61], but is mostly added to improve water solubility, sometimes interacting with an acidic side chain outside the actual ATP binding pocket. This is also the case with CK2 inhibitor **VIII** (Fig. 1), where the aminopropyl side chain addresses Asp120 [29] however, without significant impact on the potency of the parent compound TBB [30].

In general, basic functions are not common in the core structure of CK2 inhibitors targeting the ATP binding pocket of CK2, which is known for its strongly positive electrostatic potential around the conserved lysine-68, thus preferring negatively charged ligands [27]. Known CK2 ligands carrying a basic moiety are targeting the allosteric  $\alpha$ D-pocket [32] (cpd. **X**, Fig. 1), also in the selective bivalent CK2 inhibitor, AB668, which binds simultaneously the ATP site and the  $\alpha$ D pocket [36].

Importantly, the inhibitor **10b** was also able to induce cell death, whereas many of the recently developed, potent and selective CK2 inhibitors mainly inhibited the cell proliferation – which is not fully understood. Although the suppression of the analyzed CK2-dependent phosphorylations in 786-O and U937 cells by **10b** was mostly weaker than with the reference inhibitors CX-4945 or SGC-CK2-1, it was correlating with the  $GI_{50}$  and the induction of cell death. This finding can be interpreted in two ways: i) **10b** inhibits CK2 substrate phosphorylations, which are critical for tumor cell proliferation and survival, and thus impairs cell viability at the same concentrations required to

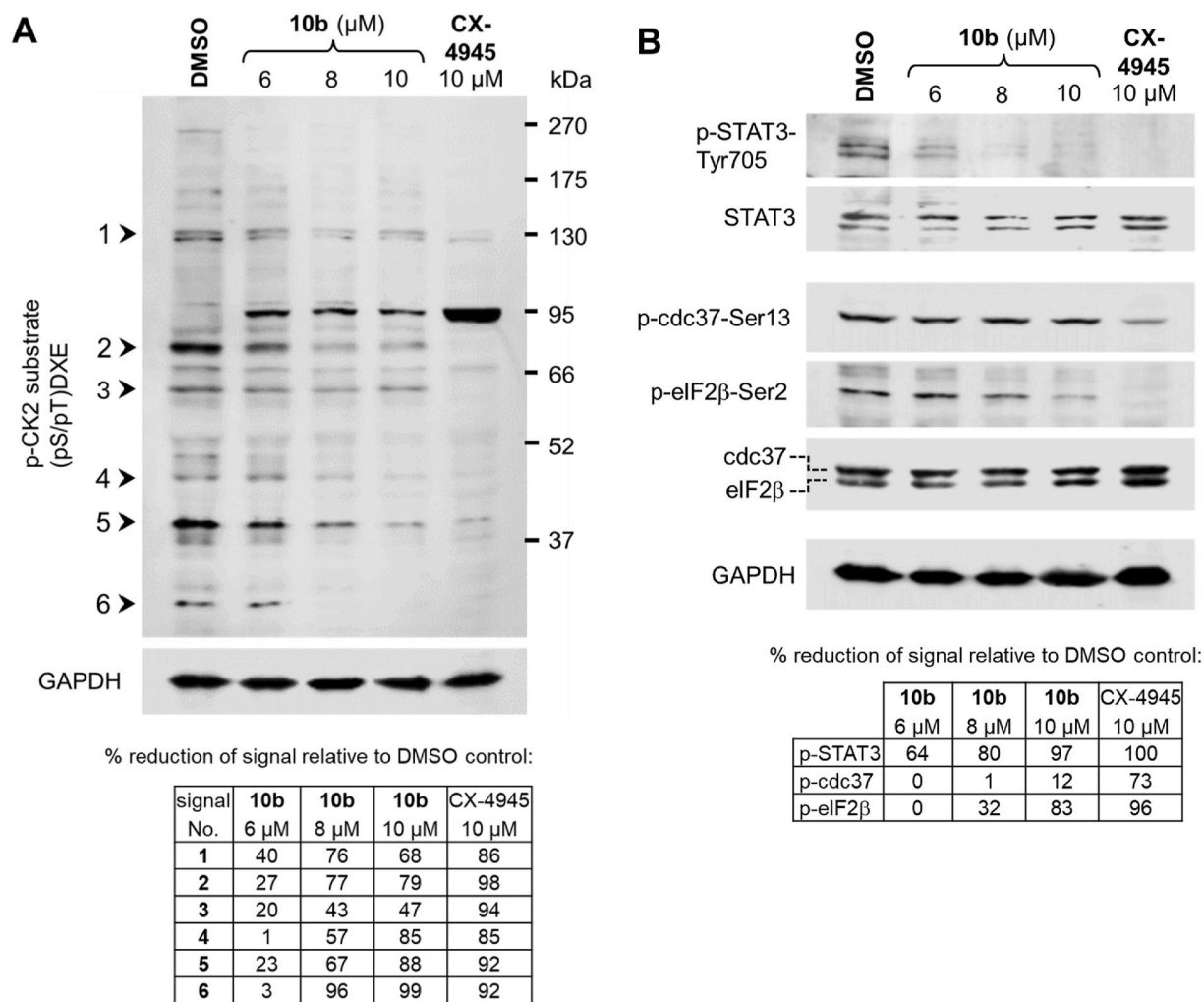


**Fig. 4.** Compound **10b** inhibits CK2-dependent protein phosphorylations in cells and induces PARP cleavage. 786-O renal cancer cells (A, B) and U937 lymphoma cells (C) were cultured in the presence of DMSO as solvent control, **10b** and reference compounds at the indicated concentrations for 48h. Total cellular proteins were then harvested and analyzed by immunoblotting. Proteins were detected using a primary antibody recognizing phosphorylated CK2-substrate motifs (A, C) or antibodies against specific phosphorylated proteins (B). Total protein of STAT3, cdc37 and eIF2β were detected for comparison. PARP cleavage was analyzed in U937 cells (C). Tables at the bottom show the % reduction of the CK2-dependent phosphorylation signals based on densitometry and in C, the ratio of cleaved PARP vs. uncleaved PARP signals. The data are representative for three (A, B) or two (C) independent experiments.

reduce the phosphorylation signals. ii) If instead a mechanism of action identical to that of CX-4945 or SGC-CK2-1 is assumed, the concentration-dependent inhibition of CK2-dependent phosphorylation in cells would be comparably weak, and an additional pharmacological activity of **10b** would likely be involved. However, the complete lack of activity against the common off-target kinases largely ruled out that co-inhibition of another protein kinase could play a role. CK2 in its native environment exists in numerous protein complexes of different binding strengths [62,63]. Such a close, permanent vicinity of the active kinase domain to the substrate creates a situation where phosphorylation of the acceptor motif is highly favored and hard to prevent by inhibitors if the complex persists. However, compounds targeting the ATP site could not only antagonize ATP binding but also modulate the protein complex network of the kinase, as shown in the seminal work by the Superti-Furga group with the c-Src and Bcr-Abl tyrosine kinases [64]. Moreover, ATP-competitive inhibitors co-crystallizing with almost indistinguishable conformations of the target kinase can still alter the conformational coupling between the two kinase lobes in solution, leading to either enhancement or disruption of the substrate binding cooperativity [65], as it was shown for the inhibitors balanol and H89,

respectively, with protein kinase A. Using NMR relaxation measurements and a model substrate peptide, balanol was shown to promote the adoption of conformationally excited states that possess enhanced binding affinity for substrates, whereas H89 blocked this conformational coupling and weakened substrate binding. Hence, a comparative analysis of the protein-protein interaction network ("interactome") or NMR studies with CK2 in the presence of SGC-CK2-1 and **10b** or other highly selective CK2 inhibitors might shed light on potential differences in the modulation of substrate binding. This might be an important factor for the efficacy of CK2 inhibitors in general and towards different subsets of CK2 substrates.

The novel basic scaffold of our lead compounds possesses a calculated pKa of 8.2 [66], which is in a range found with many marketed drugs [67]. Thus, many PK properties will be different from that of the acidic CK2 inhibitors, e.g., a larger volume of distribution could be a consequence. In addition, basic substances show greater brain exposures than acids or neutral compounds [67,68], allowing to consider brain tumors as a new indication for CK2 inhibitors.

The molecular weight is still under 400 g/mol and the polarity rather high; thus, in future optimization trials, there is room for improvement

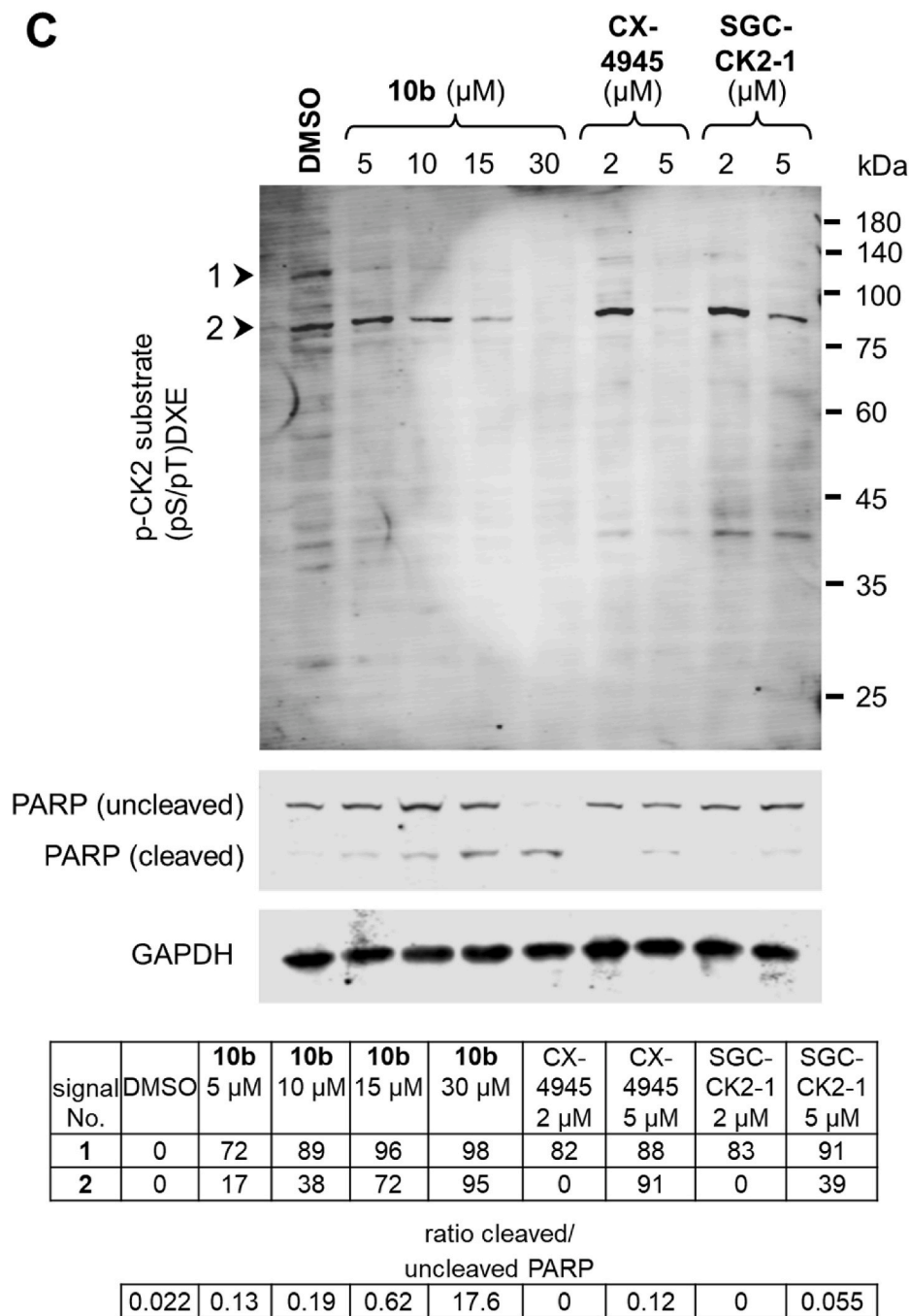
**C**

Fig. 4. (continued).

by increasing the lipophilicity. We anticipate that the presented thienopyrimidine analogs could be developed further into new therapeutical agents for CK2-driven disorders.

#### 4. Experimental section

##### 4.1. General analytical procedures for the synthesized compounds

Solvents and reagents were obtained from commercial suppliers and used without purification. Mass spectrometric analysis (HPLC-ESI-MS) was performed on a TSQ quantum (Thermo Electron Corporation) instrument equipped with an ESI source and a triple quadrupole mass detector (Thermo Finnigan, San Jose, CA). Column chromatography was carried out using silica-gel 40–60  $\mu$ M mesh. All tested compounds had a

purity of at least 95 % verified by means of HPLC coupled with mass spectrometry. HRMS was performed as previously reported [69]. A Bruker Fourier 300 spectrometer was used to obtain  $^1\text{H}$  NMR and  $^{13}\text{C}$  NMR spectra. Chemical shifts ( $\delta$ ) were reported in parts per million (ppm) by reference to the hydrogenated residues of deuterated solvent as internal standard (DMSO- $d_6$   $\delta = 2.50$  ppm ( $^1\text{H}$  NMR) and  $\delta = 39.52$  ppm ( $^{13}\text{C}$  NMR),  $\text{CDCl}_3$ :  $\delta = 7.260$  ppm ( $^1\text{H}$  NMR) and  $\delta = 77.160$  ppm ( $^{13}\text{C}$  NMR),  $(\text{CD}_3)_2\text{CO}$ :  $\delta = 2.050$  ppm ( $^1\text{H}$  NMR) and  $\delta = 29.84$  ppm and  $\delta 206.26$  ( $^{13}\text{C}$  NMR)). All coupling constants ( $J$ ) are given in Hz. Melting points were measured using Buchi B-540 melting point apparatus.

**Table 4**  
Evaluation of compound **10b** in a selectivity screen.

Kinase	Kinase % Inhibition at 2 $\mu\text{M}$ <sup>a</sup>
CK2 $\alpha$	97
CK2 $\alpha'$	57
AURKB (Aurora B)	4
CDC7/DBF4	0
CDK1/cyclin B	4
CDK2/cyclin A	3
CHEK1 (CHK1)	16
CLK3	3
CLK4	11
CSNK1G1 (CK1 $\gamma$ 1)	21
DAPK3 (ZIPK)	3
DYRK1A	4
DYRK1B	2
DYRK2	9
ERBB2 (HER2)	1
FLT3 D835Y	11
FLT4 (VEGFR3)	5
GSG2 (Haspin)	5
GSK3B (GSK3 $\beta$ )	0
HIPK1 (Myak)	5
HIPK2	15
HIPK3 (YAK1)	9
KIT D816H	4
MAPK1 (ERK2)	2
MAPK12 (p38 gamma)	5
MAPK15 (ERK7)	1
MAPK8 (JNK1)	18
MET (cMet)	2
PASK	0
PIK3CA/PIK3R1 (p110 $\alpha$ /p85 $\alpha$ )	0
PIM1	0
PRKACA (PKA)	6
PRKD1 (PKC mu)	10
RPS6KA1 (RSK1)	3
SRC	6
STK17A (DRAK1)	0
TBK1	4

<sup>a</sup> Screenings were performed as a service at ThermoFisher Scientific using ATP concentrations at the Km value. Data represent mean values of duplicates that differed by less than 10 %.

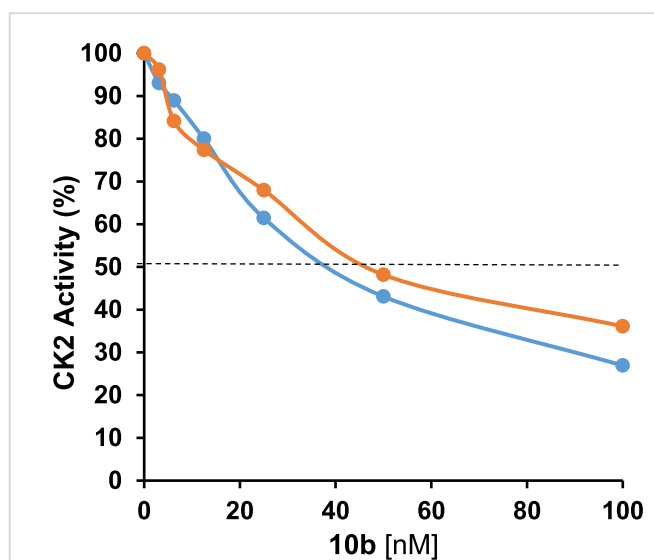


**Fig. 5.** Effects of the presence of CK2 $\beta$  on the inhibition by **10b**. CK2 $\alpha$  (36 ng) (●) or CK2 $\alpha_2\beta_2$  (40 ng) (●) were incubated in the presence of increasing concentrations of compound **10b** after which CK2 activity was measured by a radiometric assay, using a CK2 $\beta$ -independent peptide substrate. The data are representative of three independent measurements.

## 4.2. Synthesis of intermediates A-D

### 4.2.1. Synthesis of 6-(*tert*-butyl) 3-ethyl 2-amino-4,7-dihydrothieno[2,3-*c*]pyridine-3,6(5*H*)-dicarboxylate (A)

To a mixture of *tert*-butyl 4-oxopiperidine-1-carboxylate (10 mmol, 1 equiv), ethyl cyanoacetate (10 mmol, 1 equiv) and sulfur (10 mmol, 1 equiv) in absolute ethanol (10 mL), triethylamine (2 mL) was added and stirred at room temperature for 16 h. A precipitate was then produced, filtered under vacuum and washed with ethanol to give compound **A** as a white solid (87.5 %). Melting point 140.8–142 °C. <sup>1</sup>H NMR (300 MHz, CDCl<sub>3</sub>)  $\delta$  6.02 (s, 2H), 4.34 (s, 2H), 4.26 (q,  $J$  = 7.1 Hz, 2H), 3.61 (t,  $J$  = 5.7 Hz, 2H), 2.80 (s, 2H), 1.47 (s, 9H), 1.33 (t,  $J$  = 7.1 Hz, 3H). MS (ESI):  $m/z$  = 327.13 (M + H)<sup>+</sup>.

### 4.2.2. *tert*-Butyl 4-oxo-3,5,6,8-tetrahydropyrido[4',3':4,5]thieno[2,3-*d*]pyrimidine-7(4*H*)-carboxylate (B)

Intermediate **A** (10 mmol, 1 equiv) was reacted with formamidate acetate (15 mmol, 1.5 equiv) in DMF (20 mL) and heated at 100 °C for 4 days. DMF was removed under reduced pressure, and the resulting solid was thoroughly washed with water to give intermediate **B** as a yellow solid (98.5 %). Melting point 218.4–219.5 °C. <sup>1</sup>H NMR (300 MHz, CDCl<sub>3</sub>)  $\delta$  12.30 (s, 1H), 7.99 (s, 1H), 4.66 (s, 2H), 3.73 (t,  $J$  = 5.6 Hz, 2H), 3.13 (t,  $J$  = 5.5 Hz, 2H), 1.49 (s, 9H). MS (ESI):  $m/z$  = 308.13 (M + H)<sup>+</sup>.

### 4.2.3. *tert*-Butyl 4-chloro-5,8-dihydropyrido[4',3':4,5]thieno[2,3-*d*]pyrimidine-7(6*H*)-carboxylate (C)

Intermediate **B** (1 gm) was added to a mixture of POCl<sub>3</sub> (1.3 mL) and triethylamine (3.9 mL) at 0 °C. After heating the reaction mixture at 55 °C for 5 h, the reaction was cooled in iced water, and carefully neutralized using saturated aqueous sodium bicarbonate solution. Extraction of the product was done using DCM; the organic layer was separated and dried over anhydrous MgSO<sub>4</sub>, concentrated under reduced pressure, and purified by silica gel column chromatography to give intermediate **C** as a white solid (91.3 %). Melting point 156.8–158 °C. <sup>1</sup>H NMR (300 MHz, CDCl<sub>3</sub>)  $\delta$  8.76 (s, 1H), 4.74 (s, 2H), 3.79 (t,  $J$  = 5.8 Hz, 2H), 3.20 (t,  $J$  = 5.6 Hz, 2H), 1.50 (s, 9H). MS (ESI):  $m/z$  = 326.13 (M + H)<sup>+</sup>.

### 4.2.4. *tert*-Butyl 4-hydrazinyl-5,8-dihydropyrido[4',3':4,5]thieno[2,3-*d*]pyrimidine-7(6*H*)-carboxylate (D)

Hydrazine hydrate (5 equiv) was stirred with intermediate **C** (13 mmol, 1 equiv) in methanol (10 mL) and refluxed at 70 °C for 3 h. The reaction mixture was cooled, a yellow precipitate was produced which was then filtered and washed with methanol and diethyl ether to give intermediate **D** as a white solid (81.2 %). Melting point 199.7–201 °C. <sup>1</sup>H NMR (300 MHz, DMSO)  $\delta$  8.36 (s, 1H), 8.03 (s, 1H), 4.60 (s, 4H), 3.63 (t,  $J$  = 5.7 Hz, 2H), 3.00 (s, 2H), 1.43 (s, 9H). MS (ESI):  $m/z$  = 322.16 (M + H)<sup>+</sup>.

### 4.3. Procedure A: general procedure to synthesize intermediates (1a-3a) in Scheme 1

The appropriate aryl aldehyde (13 mmol) was added to a solution of intermediate **D** (11 mmol) dissolved in ethanol (15 mL) and refluxed at 80 °C overnight to give intermediates (1a-3a). The product was separated by filtration and the solid was washed several times with ethanol. The precipitate was used in the next step without further purification.

#### 4.3.1. Synthesis of *tert*-butyl 4-(2-(3-bromobenzylidene)hydrazinyl)-5,8-dihydropyrido[4',3':4,5]thieno[2,3-*d*]pyrimidine-7(6*H*)-carboxylate (1a)

The title compound was prepared according to procedure A by the reaction of intermediate **D** with 3-bromobenzaldehyde to give intermediate **1a** as a yellow solid (75.2 %). Melting point 138.2–139.7 °C. <sup>1</sup>H NMR (300 MHz, CDCl<sub>3</sub>)  $\delta$  10.46 (s, 1H), 8.28 (d,  $J$  = 8.8 Hz, 1H), 8.09–7.79 (m, 2H), 7.58 (d,  $J$  = 7.8 Hz, 1H), 7.53–7.45 (m, 1H), 7.33–7.18 (m, 1H), 4.65 (s, 2H), 3.73 (t,  $J$  = 5.5 Hz, 2H), 3.15 (t,  $J$  = 5.5

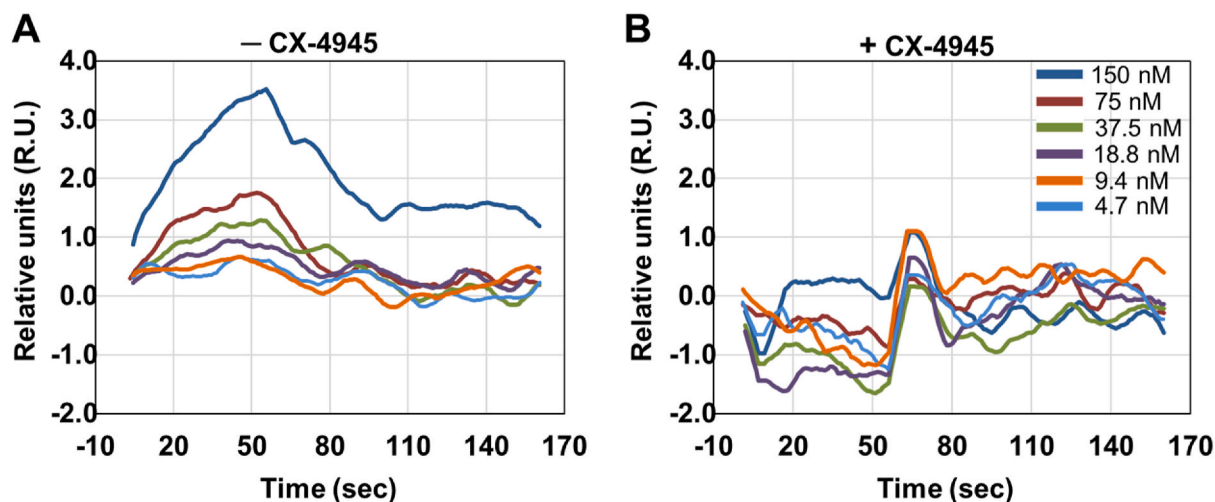


Fig. 6. SPR competition experiment with binding of **10b** to CK2 $\alpha$ . (A) In the absence of CX-4945, injection of **10b** resulted in a concentration-dependent binding to immobilized CK2 $\alpha$  on the chip surface. (B) The same experiment as in (A) was repeated with 1  $\mu$ M CX-4945 included in the running buffer, which completely abolished binding of **10b** at all concentrations.

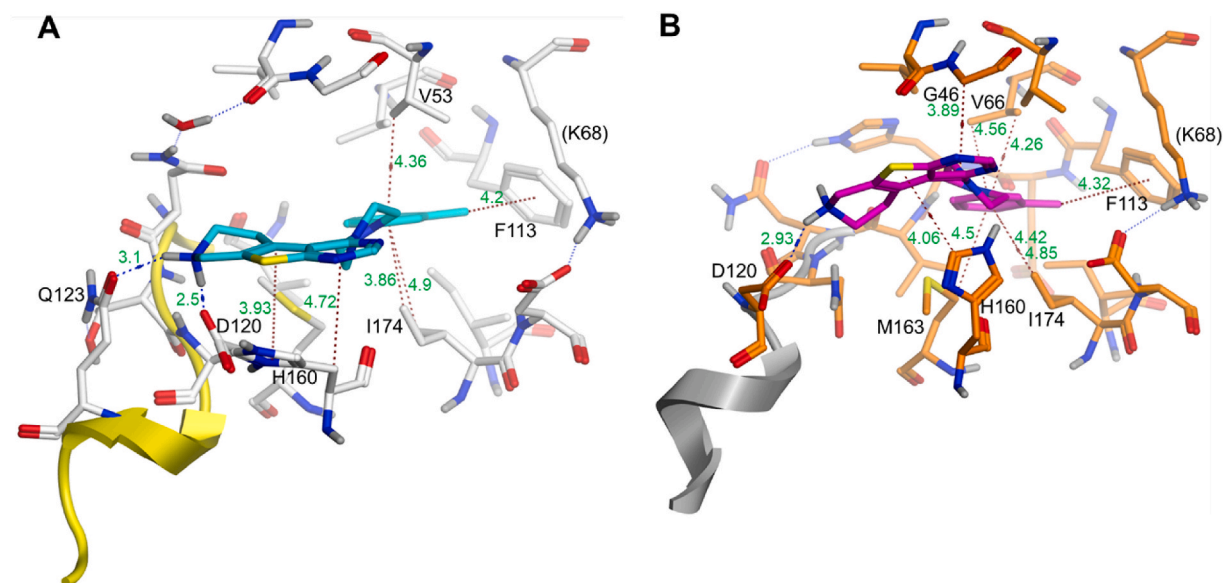


Fig. 7. Investigation of a potential binding mode by molecular docking. **12b** was docked into the ATP binding pockets of the CK2 $\alpha$  coordinates possessing a closed (PDB entry 3BQC) (A) and an open conformation (PDB entry 3Q9Y) (B), respectively, at the hinge/ $\alpha$ D region. The docking simulation predicted that **12b** preferably binds to the closed conformation (A), which corresponds to a partially inactive state. In the closed conformation (yellow loop and  $\alpha$ D-helix), optimum interactions of the protonated secondary amine can occur, involving a salt bridge with Asp120 and additionally a charge-supported H-bond with Gln123. In the open conformation (grey loop and  $\alpha$ D-helix), Gln123 is turned to the outside and not available for H-bonding with the ligand. H-bonds and salt bridges are indicated by blue dotted lines, CH- $\pi$  and  $\pi$ - $\pi$  interactions by brown dotted lines, respectively. Residues directly interacting with the ligand are indicated, and distances of the interactions are given in Å (green).

Hz, 2H), 1.50 (s, 9H). MS (ESI):  $m/z = 488.05$  (M + H) $^+$ .

#### 4.3.2. *tert*-Butyl 4-(2-(4-bromobenzylidene)hydrazinyl)-5,8-dihydropyrido[4',3':4,5]thieno[2,3-d]pyrimidine-7(6H)-carboxylate (**2a**)

The title compound was prepared according to procedure A by the reaction of intermediate **D** with 4-bromobenzaldehyde to give intermediate **2a** as a yellow solid (74.1 %). Melting point 212.6–214 °C.  $^1\text{H}$  NMR (300 MHz,  $\text{CDCl}_3$ )  $\delta$  10.39 (s, 1H), 8.35 (s, 1H), 7.68 (t,  $J = 11.7$  Hz, 1H), 7.59 (t,  $J = 7.5$  Hz, 2H), 7.50 (d,  $J = 7.8$  Hz, 2H), 4.66 (s, 2H), 3.73 (s, 2H), 3.15 (s, 2H), 1.50 (s, 9H).  $^{13}\text{C}$  NMR (75 MHz,  $\text{CDCl}_3$ )  $\delta$  161.31, 154.73, 133.04, 132.25, 132.07, 130.07, 129.10, 128.28, 127.29, 125.97, 124.61, 124.52, 80.56, 43.22, 41.69, 28.58, 26.96. MS (ESI):  $m/z = 488.02$  (M + H) $^+$ .

#### 4.3.3. *tert*-Butyl 4-(2-(naphthalen-1-ylmethylene)hydrazinyl)-5,8-dihydropyrido[4',3':4,5]thieno[2,3-d]pyrimidine-7(6H)-carboxylate (**3a**)

The title compound was prepared according to procedure A by the reaction of intermediate **D** with 1-naphthaldehyde to give intermediate **3a** as a yellow solid (95.1 %). Melting point 120.7–122 °C.

$^1\text{H}$  NMR (300 MHz,  $\text{CDCl}_3$ )  $\delta$  10.44 (s, 1H), 9.11 (s, 1H), 8.65–8.55 (m, 1H), 8.04 (d,  $J = 7.2$  Hz, 1H), 7.89 (d,  $J = 8.1$  Hz, 2H), 7.74–7.45 (m, 4H), 4.67 (s, 2H), 3.74 (d,  $J = 5.1$  Hz, 2H), 3.20 (s, 2H), 1.54–1.46 (m, 9H). MS (ESI):  $m/z = 460.16$  (M + H) $^+$ .

#### 4.4. Procedure B: general procedure to synthesize intermediates (4a-16a) in Scheme 2

The appropriate amine (1.1 mmol) was added to a solution of intermediate **C** (0.7 mmol) dissolved in ethanol (7 mL) and refluxed at 80 °C overnight. The solvent was removed under reduced pressure, and the remaining residue was partitioned between water and EtOAc; the organic layer was separated, dried over anhydrous MgSO<sub>4</sub>, concentrated, and purified by silica gel column chromatography to give intermediates (4a-16a).

##### 4.4.1. Synthesis of tert-butyl 4-(4-acetylpiperazin-1-yl)-5,8-dihydropyrido[4',3':4,5]thieno[2,3-d]pyrimidine-7(6H)-carboxylate (4a)

The title compound was prepared according to procedure B by the reaction of intermediate **C** with 1-acetylpiperazine to give intermediate **4a** as a white solid (77.4 %). Melting point 102.6–103.8 °C. <sup>1</sup>H NMR (300 MHz, CDCl<sub>3</sub>) δ 8.56 (d, *J* = 9.0 Hz, 1H), 4.71 (s, 2H), 3.81–3.72 (m, 2H), 3.65 (dd, *J* = 8.2, 5.3 Hz, 4H), 3.46 (s, 2H), 3.43–3.33 (m, 2H), 3.02 (s, 2H), 2.14 (s, 3H), 1.51 (s, 9H). <sup>13</sup>C NMR (75 MHz, CDCl<sub>3</sub>) δ 169.21, 168.85, 161.79, 154.42, 151.94, 125.81, 120.48, 80.63, 50.60, 49.94, 45.81, 41.01, 28.40, 27.02, 21.33. MS (ESI): *m/z* = 418.10 (M + H)<sup>+</sup>.

##### 4.4.2. tert-Butyl 4-(4-(methylsulfonyl)piperazin-1-yl)-5,8-dihydropyrido[4',3':4,5]thieno[2,3-d]pyrimidine-7(6H)-carboxylate (5a)

The title compound was prepared according to procedure B by the reaction of intermediate **C** with 1-(methylsulfonyl)piperazine to give intermediate **5a** as a white solid (66 %). Melting point 175.1–176.5 °C. <sup>1</sup>H NMR (300 MHz, CDCl<sub>3</sub>) δ 8.55 (s, 1H), 4.72 (s, 2H), 3.68 (t, *J* = 5.0 Hz, 2H), 3.58 (s, 4H), 3.42–3.32 (m, 4H), 3.01 (s, 2H), 2.83 (s, 3H), 1.51 (s, 9H). <sup>13</sup>C NMR (75 MHz, CDCl<sub>3</sub>) δ 169.16, 162.66, 161.62, 154.57, 152.07, 125.95, 120.56, 80.84, 50.06, 45.36, 36.58, 35.02, 31.53, 28.57, 27.19. MS (ESI): *m/z* = 454.06 (M + H)<sup>+</sup>.

##### 4.4.3. tert-Butyl 4-(4-phenylpiperazin-1-yl)-5,8-dihydropyrido[4',3':4,5]thieno[2,3-d]pyrimidine-7(6H)-carboxylate (6a)

The title compound was prepared according to procedure B by the reaction of intermediate **C** with 1-phenylpiperazine to give intermediate **6a** as a yellow solid (77.1 %). Melting point 118.2–119.5 °C. <sup>1</sup>H NMR (300 MHz, DMSO) δ 8.54 (s, 1H), 7.24 (dd, *J* = 8.6, 7.3 Hz, 2H), 7.00 (d, *J* = 7.9 Hz, 2H), 6.82 (t, *J* = 7.2 Hz, 1H), 4.69 (s, 2H), 4.03 (q, *J* = 7.1 Hz, 2H), 3.59 (t, *J* = 5.2 Hz, 2H), 3.53 (s, 4H), 3.04 (s, 2H), 1.99 (s, 2H), 1.46 (s, 9H). <sup>13</sup>C NMR (75 MHz, DMSO-*d*<sub>6</sub>) δ 167.85, 161.43, 153.75, 151.77, 150.92, 128.96, 126.41, 126.23, 119.47, 119.24, 115.72, 79.50, 59.72, 49.81, 48.08, 28.07, 26.82. MS (ESI): *m/z* = 452.24 (M + H)<sup>+</sup>.

##### 4.4.4. tert-Butyl 4-(4-(2-fluorophenyl)piperazin-1-yl)-5,8-dihydropyrido[4',3':4,5]thieno[2,3-d]pyrimidine-7(6H)-carboxylate (7a)

The title compound was prepared according to procedure B by the reaction of intermediate **C** with 1-(2-fluorophenyl)piperazine to give intermediate **7a** as a white solid (90.6 %). Melting point 83.7–85 °C. <sup>1</sup>H NMR (300 MHz, CDCl<sub>3</sub>) δ 8.57 (s, 1H), 7.11 (dd, *J* = 8.3, 1.4 Hz, 1H), 7.06 (d, *J* = 6.2 Hz, 1H), 7.01 (dd, *J* = 6.4, 2.8 Hz, 1H), 6.99–6.93 (m, 1H), 4.72 (s, 2H), 3.68 (s, 2H), 3.66–3.59 (m, 4H), 3.31–3.20 (m, 4H), 3.08 (s, 2H), 1.52 (s, 9H). <sup>13</sup>C NMR (75 MHz, CDCl<sub>3</sub>) δ 168.85, 162.20, 155.90 (d, *J* = 246.1 Hz), 154.65 (d, *J* = 2.8 Hz), 152.16, 139.88 (d, *J* = 8.4 Hz), 130.02, 126.35, 124.68, 123.06 (d, *J* = 8.6 Hz), 120.47 (d, *J* = 2.7 Hz), 119.27, 116.39 (d, *J* = 20.9 Hz), 80.71, 50.60, 50.44, 44.32, 40.81, 28.58, 27.44. MS (ESI): *m/z* = 470.11 (M + H)<sup>+</sup>.

##### 4.4.5. tert-Butyl 4-(4-(3-fluorophenyl)piperazin-1-yl)-5,8-dihydropyrido[4',3':4,5]thieno[2,3-d]pyrimidine-7(6H)-carboxylate (8a)

The title compound was prepared according to procedure B by the reaction of intermediate **C** with 1-(3-fluorophenyl)piperazine to give intermediate **8a** as a white solid (80.5 %). Melting point 119.6–121.1 °C. <sup>1</sup>H NMR (300 MHz, CDCl<sub>3</sub>) δ 8.58 (s, 1H), 7.21 (dd, *J* = 8.1, 7.1 Hz, 1H), 6.73 (dd, *J* = 8.3, 2.1 Hz, 1H), 6.65 (dt, *J* = 12.2, 2.3 Hz, 1H), 6.58 (td, *J*

= 8.2, 2.3 Hz, 1H), 4.73 (s, 2H), 3.68 (d, *J* = 4.9 Hz, 2H), 3.62–3.53 (m, 4H), 3.40–3.32 (m, 4H), 3.08 (s, 2H), 1.52 (s, 9H). MS (ESI): *m/z* = 470.20 (M + H)<sup>+</sup>.

##### 4.4.6. tert-Butyl 4-(4-(4-fluorophenyl)piperazin-1-yl)-5,8-dihydropyrido[4',3':4,5]thieno[2,3-d]pyrimidine-7(6H)-carboxylate (9a)

The title compound was prepared according to procedure B by the reaction of intermediate **C** with 1-(4-fluorophenyl)piperazine to give intermediate **9a** as a white solid (90 %). Melting point 158.5–160 °C. <sup>1</sup>H NMR (300 MHz, CDCl<sub>3</sub>) δ 8.51 (s, 1H), 6.98–6.90 (m, 2H), 6.90–6.83 (m, 2H), 4.66 (s, 2H), 3.61 (d, *J* = 4.7 Hz, 2H), 3.57–3.47 (m, 4H), 3.30–3.15 (m, 4H), 3.01 (s, 2H), 1.45 (s, 9H). MS (ESI): *m/z* = 470.11 (M + H)<sup>+</sup>.

##### 4.4.7. tert-Butyl 4-(4-(4-chlorophenyl)piperazin-1-yl)-5,8-dihydropyrido[4',3':4,5]thieno[2,3-d]pyrimidine-7(6H)-carboxylate (10a)

The title compound was prepared according to procedure B by the reaction of intermediate **C** with 1-(4-chlorophenyl)piperazine to give intermediate **10a** as a white solid (48.2 %). Melting point 155.3–156.8 °C. <sup>1</sup>H NMR (300 MHz, CDCl<sub>3</sub>) δ 8.58 (s, 1H), 7.26–7.22 (m, 2H), 6.96–6.84 (m, 2H), 4.73 (s, 2H), 3.68 (s, 2H), 3.62–3.53 (m, 4H), 3.37–3.27 (m, 4H), 3.08 (s, 2H), 1.52 (s, 9H). MS (ESI): *m/z* = 486.16 (M + H)<sup>+</sup>.

##### 4.4.8. tert-Butyl 4-(4-(*o*-tolyl)piperazin-1-yl)-5,8-dihydropyrido[4',3':4,5]thieno[2,3-d]pyrimidine-7(6H)-carboxylate (11a)

The title compound was prepared according to procedure B by the reaction of intermediate **C** with 1-(2-methylphenyl)piperazine to give intermediate **11a** as a white solid (79 %). Melting point 83.6–84.8 °C. <sup>1</sup>H NMR (300 MHz, CDCl<sub>3</sub>) δ 8.57 (s, 1H), 7.20 (t, *J* = 7.3 Hz, 2H), 7.06 (d, *J* = 10.5 Hz, 1H), 7.01 (d, *J* = 7.1 Hz, 1H), 4.73 (s, 2H), 3.69 (s, 2H), 3.61 (s, 4H), 3.09 (d, *J* = 4.3 Hz, 6H), 2.35 (s, 3H), 1.52 (s, 9H). MS (ESI): *m/z* = 466.13 (M + H)<sup>+</sup>.

##### 4.4.9. tert-Butyl 4-(4-(*m*-tolyl)piperazin-1-yl)-5,8-dihydropyrido[4',3':4,5]thieno[2,3-d]pyrimidine-7(6H)-carboxylate (12a)

The title compound was prepared according to procedure B by the reaction of intermediate **C** with 1-(3-methylphenyl)piperazine to give intermediate **12a** as a white solid (95.7 %). Melting point 90.6–91.7 °C. <sup>1</sup>H NMR (300 MHz, CDCl<sub>3</sub>) δ 8.57 (s, 1H), 7.19 (t, *J* = 7.9 Hz, 1H), 6.80 (d, *J* = 7.3 Hz, 2H), 6.74 (d, *J* = 7.4 Hz, 1H), 4.73 (s, 2H), 3.68 (s, 2H), 3.64–3.52 (m, 4H), 3.42–3.26 (m, 4H), 3.09 (s, 2H), 2.35 (s, 3H), 1.53 (s, 9H). MS (ESI): *m/z* = 466.13 (M + H)<sup>+</sup>.

##### 4.4.10. tert-Butyl 4-(4-(*p*-tolyl)piperazin-1-yl)-5,8-dihydropyrido[4',3':4,5]thieno[2,3-d]pyrimidine-7(6H)-carboxylate (13a)

The title compound was prepared according to procedure B by the reaction of intermediate **C** with 1-(4-methylphenyl)piperazine to give intermediate **13a** as a white solid (67.7 %). Melting point 186–188 °C. <sup>1</sup>H NMR (300 MHz, CDCl<sub>3</sub>) δ 8.57 (s, 1H), 7.11 (d, *J* = 8.5 Hz, 2H), 6.90 (d, *J* = 8.4 Hz, 2H), 4.72 (s, 2H), 3.68 (s, 2H), 3.63–3.52 (m, 4H), 3.38–3.22 (m, 4H), 3.08 (s, 2H), 2.29 (s, 3H), 1.52 (s, 9H). MS (ESI): *m/z* = 466.25 (M + H)<sup>+</sup>.

##### 4.4.11. tert-Butyl 4-(4-(2-methoxyphenyl)piperazin-1-yl)-5,8-dihydropyrido[4',3':4,5]thieno[2,3-d]pyrimidine-7(6H)-carboxylate (14a)

The title compound was prepared according to procedure B by the reaction of intermediate **C** with 1-(2-methoxyphenyl)piperazine to give intermediate **14a** as a white solid (94.9 %). Melting point 166.6–168.2 °C. <sup>1</sup>H NMR (300 MHz, (CD<sub>3</sub>)<sub>2</sub>CO) δ 8.49 (s, 1H), 7.02–6.94 (m, 3H), 6.90 (ddd, *J* = 7.2, 6.0, 3.0 Hz, 1H), 4.75 (s, 2H), 3.86 (s, 3H), 3.70 (t, *J* = 5.3 Hz, 2H), 3.65–3.54 (m, 4H), 3.30–3.18 (m, 4H), 3.14 (t, *J* = 5.5 Hz, 2H), 1.49 (s, 9H). MS (ESI): *m/z* = 482.22 (M + H)<sup>+</sup>.

##### 4.4.12. tert-Butyl 4-(4-(3-methoxyphenyl)piperazin-1-yl)-5,8-dihydropyrido[4',3':4,5]thieno[2,3-d]pyrimidine-7(6H)-carboxylate (15a)

The title compound was prepared according to procedure B by the

reaction of intermediate **C** with 1-(3-methoxyphenyl)piperazine to give intermediate **15a** as a white solid (70.7 %). Melting point 184.9–186 °C. <sup>1</sup>H NMR (300 MHz, CDCl<sub>3</sub>) δ 8.57 (s, 1H), 7.21 (t, *J* = 8.2 Hz, 1H), 6.60 (d, *J* = 8.2 Hz, 1H), 6.52 (s, 1H), 6.47 (dd, *J* = 8.1, 2.2 Hz, 1H), 4.73 (s, 2H), 3.81 (s, 3H), 3.68 (s, 2H), 3.63–3.53 (m, 4H), 3.41–3.25 (m, 4H), 3.08 (s, 2H), 1.52 (s, 9H). <sup>13</sup>C NMR (75 MHz, CDCl<sub>3</sub>) δ 169.15, 162.49, 161.08, 154.91, 152.86, 152.48, 131.84, 130.34, 126.59, 120.86, 109.50, 105.57, 103.19, 81.01, 55.66, 50.73, 49.47, 44.57, 41.09, 28.87, 27.71. MS (ESI): *m/z* = 482.20 (M + H)<sup>+</sup>.

#### 4.4.13. *tert*-Butyl 4-(4-(4-methoxyphenyl)piperazin-1-yl)-5,8-dihydropyrido[4',3':4,5]thieno[2,3-d]pyrimidine-7(6H)-carboxylate (**16a**)

The title compound was prepared according to procedure B by the reaction of intermediate **C** with 1-(4-methoxyphenyl)piperazine to give intermediate **16a** as a white solid (81 %). Melting point 182.9–184 °C. <sup>1</sup>H NMR (300 MHz, CDCl<sub>3</sub>) δ 8.57 (s, 1H), 6.96 (d, *J* = 9.0 Hz, 2H), 6.87 (d, *J* = 9.2 Hz, 2H), 4.72 (s, 2H), 3.78 (s, 3H), 3.68 (s, 2H), 3.64–3.55 (m, 4H), 3.29–3.19 (m, 4H), 3.08 (s, 2H), 1.52 (s, 9H). MS (ESI): *m/z* = 482.10 (M + H)<sup>+</sup>.

### 4.5. Procedure C: general procedure to synthesize compounds (**1b–16b**) in Schemes 1 and 2

Trifluoroacetic acid (1 mL) was added to a mixture of intermediate (**1a–16a**) and DCM (2 mL) at 0 °C, then reaction was left to attain room temperature and stirred for 4 h. All volatiles were removed under vacuum. Several aliquots of DCM and diethyl ether were added to the residue few times and evaporated to ensure complete evaporation of TFA to give compounds (**1b–16b**) as trifluoroacetic salts.

#### 4.5.1. Synthesis of 4-(2-(3-bromobenzylidene)hydrazinyl)-5,6,7,8-tetrahydropyrido[4',3':4,5]thieno[2,3-d]pyrimidin-7-ium 2,2,2-trifluoroacetate (**1b**)

The title compound was prepared by BOC-deprotection of intermediate **1a** according to procedure C to give compound **1b** as a white solid (94.1 %). Melting point 215–216 °C. <sup>1</sup>H NMR (300 MHz, DMSO-*d*<sub>6</sub>) δ 9.33 (s, 2H), 8.39 (s, 1H), 8.27 (s, 1H), 7.95 (s, 1H), 7.87 (d, *J* = 7.8 Hz, 1H), 7.61 (d, *J* = 7.9 Hz, 1H), 7.42 (t, *J* = 7.8 Hz, 1H), 4.43 (s, 2H), 3.45 (s, 2H), 3.27 (s, 2H). <sup>13</sup>C NMR (75 MHz, DMSO-*d*<sub>6</sub>) δ 158.35 (q, *J* = 34.9 Hz), 151.66, 149.43, 145.50, 137.62, 132.37, 130.71, 129.42, 128.00, 127.30, 124.39, 122.24, 117.71, 116.10 (q, *J* = 293.9 Hz), 114.16, 46.04, 41.62, 23.67. MS (ESI): *m/z* = 387.96 (M + H)<sup>+</sup>. HRMS (ESI+) *m/z* calcd. for C<sub>16</sub>H<sub>15</sub>BrN<sub>5</sub>S<sup>+</sup> (M + H)<sup>+</sup>: 388.0227 found 388.0222.

#### 4.5.2. 4-(2-(4-Bromobenzylidene)hydrazinyl)-5,6,7,8-tetrahydropyrido[4',3':4,5]thieno[2,3-d]pyrimidin-7-ium 2,2,2-trifluoroacetate (**2b**)

The title compound was prepared by BOC-deprotection of intermediate **2a** according to procedure C to give compound **2b** as a white solid (97.7 %). Melting point 243.6–245 °C. <sup>1</sup>H NMR (300 MHz, DMSO) δ 9.39 (s, 2H), 8.38 (s, 1H), 8.26 (t, *J* = 1.5 Hz, 1H), 7.94 (s, 1H), 7.86 (d, *J* = 7.8 Hz, 1H), 7.60 (ddd, *J* = 8.0, 2.0, 1.0 Hz, 1H), 7.40 (t, *J* = 7.8 Hz, 1H), 4.42 (s, 2H), 3.44 (s, 2H), 3.26 (d, *J* = 5.3 Hz, 2H). <sup>13</sup>C NMR (75 MHz, DMSO-*d*<sub>6</sub>) δ 158.38 (q, *J* = 35.1 Hz), 151.87, 149.38, 145.68, 134.43, 131.57, 129.60, 127.95, 124.35, 123.18, 117.66, 116.06 (q, *J* = 290.7 Hz), 114.12, 41.62, 40.45, 23.67. MS (ESI): *m/z* = 388.00 (M + H)<sup>+</sup>. HRMS (ESI+) *m/z* calcd. for C<sub>16</sub>H<sub>15</sub>BrN<sub>5</sub>S<sup>+</sup> (M + H)<sup>+</sup>: 388.0227 found 388.0221.

#### 4.5.3. 4-(2-(Naphthalen-1-ylmethylene)hydrazinyl)-5,6,7,8-tetrahydropyrido[4',3':4,5]thieno[2,3-d]pyrimidin-7-ium 2,2,2-trifluoroacetate (**3b**)

The title compound was prepared by BOC-deprotection of intermediate **3a** according to procedure C to give compound **3b** as a yellow solid (94.9 %). Melting point 251.8–253 °C. <sup>1</sup>H NMR (300 MHz, DMSO-*d*<sub>6</sub>) δ 9.35 (s, 2H), 9.18 (s, 1H), 8.67 (d, *J* = 7.9 Hz, 1H), 8.36 (d, *J* = 7.2 Hz, 1H), 8.05 (s, 1H), 8.02 (s, 1H), 8.00 (s, 1H), 7.69–7.64 (m, 1H), 7.62 (s,

1H), 7.59 (d, *J* = 6.3 Hz, 1H), 4.44 (s, 2H), 3.47 (s, 2H), 3.41–3.23 (m, 2H). MS (ESI): *m/z* = 360.15 (M + H)<sup>+</sup>. HRMS (ESI+) *m/z* calcd. for C<sub>20</sub>H<sub>18</sub>N<sub>5</sub>S<sup>+</sup> (M + H)<sup>+</sup>: 360.1278 found 360.1271.

#### 4.5.4. 4-(4-Acetylpiperazin-1-yl)-5,6,7,8-tetrahydropyrido[4',3':4,5]thieno[2,3-d]pyrimidin-7-ium 2,2,2-trifluoroacetate (**4b**)

The title compound was prepared by BOC-deprotection of intermediate **4a** according to procedure C to give compound **4b** as a yellow oily liquid (73.6 %). <sup>1</sup>H NMR (300 MHz, DMSO-*d*<sub>6</sub>) δ 9.43 (s, 2H), 8.60 (s, 1H), 4.51 (s, 2H), 3.65–3.59 (m, 4H), 3.40 (d, *J* = 7.0 Hz, 4H), 3.33 (d, *J* = 8.0 Hz, 2H), 3.19 (d, *J* = 5.2 Hz, 2H), 2.06 (s, 3H). <sup>13</sup>C NMR (75 MHz, DMSO-*d*<sub>6</sub>) δ 168.59, 168.02, 161.82, 158.38 (q, *J* = 36.8 Hz), 152.28, 126.65, 124.98, 119.09, 115.55 (q, *J* = 291.0 Hz), 50.34, 45.14, 42.09, 40.78, 23.16, 21.24. MS (ESI): *m/z* = 318.13 (M + H)<sup>+</sup>. HRMS (ESI+) *m/z* calcd. for C<sub>15</sub>H<sub>20</sub>N<sub>5</sub>OS<sup>+</sup> (M + H)<sup>+</sup>: 318.1384 found 318.1380.

#### 4.5.5. 4-(4-(Methylsulfonyl)piperazin-1-yl)-5,6,7,8-tetrahydropyrido[4',3':4,5]thieno[2,3-d]pyrimidin-7-ium 2,2,2-trifluoroacetate (**5b**)

The title compound was prepared by BOC-deprotection of intermediate **5a** according to procedure C to give compound **5b** as a yellow oily liquid (98.6 %). <sup>1</sup>H NMR (300 MHz, DMSO-*d*<sub>6</sub>) δ 9.44 (s, 2H), 8.61 (s, 1H), 4.52 (s, 2H), 3.47 (d, *J* = 5.2 Hz, 4H), 3.40 (d, *J* = 7.0 Hz, 2H), 3.33 (d, *J* = 4.9 Hz, 4H), 3.18 (d, *J* = 5.2 Hz, 2H), 2.96 (s, 3H). <sup>13</sup>C NMR (75 MHz, DMSO-*d*<sub>6</sub>) δ 168.61, 162.09, 158.82 (q, *J* = 36.0 Hz), 152.75, 127.30, 125.39, 119.56, 116.13 (q, *J* = 291.6 Hz), 50.13, 45.37, 42.57, 41.24, 34.76, 23.60. MS (ESI): *m/z* = 354.06 (M + H)<sup>+</sup>. HRMS (ESI+) *m/z* calcd. for C<sub>14</sub>H<sub>20</sub>N<sub>5</sub>O<sub>2</sub>S<sub>2</sub><sup>+</sup> (M + H)<sup>+</sup>: 354.1053 found 354.1049.

#### 4.5.6. 4-(4-Phenylpiperazin-1-yl)-5,6,7,8-tetrahydropyrido[4',3':4,5]thieno[2,3-d]pyrimidin-7-ium 2,2,2-trifluoroacetate (**6b**)

The title compound was prepared by BOC-deprotection of intermediate **6a** according to procedure C to give compound **6b** as a yellow solid (73.5 %). Melting point 187.4–189 °C. <sup>1</sup>H NMR (300 MHz, CDCl<sub>3</sub>) δ 8.58 (s, 1H), 7.30 (dd, *J* = 8.7, 7.3 Hz, 2H), 7.02–6.94 (m, 2H), 6.91 (t, *J* = 7.3 Hz, 1H), 4.22 (s, 2H), 3.65–3.54 (m, 4H), 3.42–3.28 (m, 4H), 3.17 (t, *J* = 5.3 Hz, 2H), 3.07 (d, *J* = 5.0 Hz, 2H). <sup>13</sup>C NMR (75 MHz, CDCl<sub>3</sub>) δ 168.70, 162.42, 152.11, 151.27, 133.14, 129.37, 125.96, 121.13, 120.46, 116.52, 50.70, 49.27, 45.38, 43.29, 27.75. MS (ESI): *m/z* = 352.23 (M + H)<sup>+</sup>. HRMS (ESI+) *m/z* calcd. for C<sub>19</sub>H<sub>22</sub>N<sub>5</sub>S<sup>+</sup> (M + H)<sup>+</sup>: 352.1591 found 352.1583.

#### 4.5.7. 4-(2-(2-Fluorophenyl)piperazin-1-yl)-5,6,7,8-tetrahydropyrido[4',3':4,5]thieno[2,3-d]pyrimidin-7-ium 2,2,2-trifluoroacetate (**7b**)

The title compound was prepared by BOC-deprotection of intermediate **7a** according to procedure C to give compound **7b** as a yellow oily liquid (93.4 %). <sup>1</sup>H NMR (300 MHz, DMSO-*d*<sub>6</sub>) δ 9.42 (s, 2H), 8.61 (s, 1H), 7.19 (d, *J* = 7.7 Hz, 1H), 7.17–7.14 (m, 1H), 7.13 (s, *J* = 4.0 Hz, 1H), 7.04–6.97 (m, 1H), 4.52 (s, 2H), 3.55 (s, 4H), 3.41 (d, *J* = 10.4 Hz, 2H), 3.22 (s, 6H). <sup>13</sup>C NMR (75 MHz, DMSO) δ 168.00, 160.19 (d, *J* = 247.4 Hz), 152.32, 139.63 (d, *J* = 5.1 Hz), 139.49, 126.53, 125.04, 122.84 (d, *J* = 8.1 Hz), 119.52 (d, *J* = 2.8 Hz), 119.00, 117.70, 116.01 (d, *J* = 14.4 Hz), 50.17, 49.74 (d, *J* = 3.4 Hz), 42.10, 40.81, 23.29. MS (ESI): *m/z* = 370.10 (M + H)<sup>+</sup>. HRMS (ESI+) *m/z* calcd. for C<sub>19</sub>H<sub>21</sub>FN<sub>5</sub>S<sup>+</sup> (M + H)<sup>+</sup>: 370.1497 found 370.1491.

#### 4.5.8. 4-(4-(3-Fluorophenyl)piperazin-1-yl)-5,6,7,8-tetrahydropyrido[4',3':4,5]thieno[2,3-d]pyrimidin-7-ium 2,2,2-trifluoroacetate (**8b**)

The title compound was prepared by BOC-deprotection of intermediate **8a** according to procedure C to give compound **8b** as a white solid (89.5 %). Melting point 226.8–228 °C. <sup>1</sup>H NMR (300 MHz, DMSO-*d*<sub>6</sub>) δ 9.47 (s, 2H), 8.62 (s, 1H), 7.26 (dd, *J* = 15.9, 7.9 Hz, 1H), 6.86 (d, *J* = 1.2 Hz, 1H), 6.84–6.80 (m, 1H), 6.65–6.54 (m, 1H), 4.52 (s, 2H), 3.50 (d, *J* = 4.8 Hz, 4H), 3.40 (dd, *J* = 10.9, 6.2 Hz, 6H), 3.21 (s, 2H). <sup>13</sup>C NMR (75 MHz, DMSO) δ 168.01, 163.38 (d, *J* = 222.1 Hz), 163.24, 152.65 (d, *J* = 10.0 Hz), 152.35, 130.40 (d, *J* = 10.2 Hz), 126.65, 125.00, 119.14, 111.19 (d, *J* = 2.1 Hz), 105.21 (d, *J* = 21.0 Hz), 102.16 (d, *J* = 25.0 Hz),

49.87, 47.40, 42.07, 40.77, 23.27. MS (ESI):  $m/z = 370.14$  (M + H)<sup>+</sup>. HRMS (ESI+)  $m/z$  calcd. for C<sub>19</sub>H<sub>21</sub>FN<sub>5</sub>S<sup>+</sup> (M + H)<sup>+</sup>: 370.1497 found 370.1490.

**4.5.9. 4-(4-(4-Fluorophenyl)piperazin-1-yl)-5,6,7,8-tetrahydropyrido[4',3':4,5]thieno[2,3-d]pyrimidin-7-ium 2,2,2-trifluoroacetate (9b)**

The title compound was prepared by BOC-deprotection of intermediate **9a** according to procedure C to give compound **9b** as a white solid (96.9 %). Melting point 181.5–183 °C. <sup>1</sup>H NMR (300 MHz, (CD<sub>3</sub>)<sub>2</sub>CO) δ 8.58 (s, 1H), 7.12–7.07 (m, 2H), 7.07–7.01 (m, 2H), 4.80 (s, 2H), 3.77 (t,  $J = 5.8$  Hz, 2H), 3.68–3.60 (m, 4H), 3.55 (t,  $J = 5.8$  Hz, 2H), 3.43–3.32 (m, 4H). <sup>13</sup>C NMR (75 MHz, (CD<sub>3</sub>)<sub>2</sub>CO) δ 169.33, 165.60, 161.38 (d,  $J = 279.8$  Hz), 153.15, 148.60 (d,  $J = 2.3$  Hz), 127.12, 126.21, 120.41, 118.89 (d,  $J = 7.6$  Hz), 115.96 (d,  $J = 22.2$  Hz), 51.07, 50.33, 43.11, 42.16, 24.21. MS (ESI):  $m/z = 370.14$  (M + H)<sup>+</sup>. HRMS (ESI+)  $m/z$  calcd. for C<sub>19</sub>H<sub>21</sub>FN<sub>5</sub>S<sup>+</sup> (M + H)<sup>+</sup>: 370.1497 found 370.1491.

**4.5.10. 4-(4-(4-Chlorophenyl)piperazin-1-yl)-5,6,7,8-tetrahydropyrido[4',3':4,5]thieno[2,3-d]pyrimidin-7-ium 2,2,2-trifluoroacetate (10b)**

The title compound was prepared by BOC-deprotection of intermediate **10a** according to procedure C to give compound **10b** as a yellow solid (97.8 %). Melting point 204.8–206.3 °C. <sup>1</sup>H NMR (300 MHz, DMSO-*d*<sub>6</sub>) δ 9.44 (s, 2H), 8.62 (s, 1H), 7.38–7.17 (m, 2H), 7.04 (t,  $J = 6.2$  Hz, 2H), 4.52 (s, 2H), 3.50 (d,  $J = 5.1$  Hz, 4H), 3.42 (s, 2H), 3.35 (d,  $J = 4.9$  Hz, 4H), 3.19 (d,  $J = 12.3$  Hz, 2H). <sup>13</sup>C NMR (75 MHz, DMSO-*d*<sub>6</sub>) δ 168.49, 162.41, 152.84, 150.17, 129.18, 127.12, 125.50, 123.37, 119.62, 117.72, 50.43, 48.26, 42.59, 41.28, 23.75. MS (ESI):  $m/z = 386.13$  (M + H)<sup>+</sup>. HRMS (ESI+)  $m/z$  calcd. for C<sub>19</sub>H<sub>21</sub>ClN<sub>5</sub>S<sup>+</sup> (M + H)<sup>+</sup>: 386.1201 found 386.1195.

**4.5.11. 4-(4-(*o*-tolyl)piperazin-1-yl)-5,6,7,8-tetrahydropyrido[4',3':4,5]thieno[2,3-d]pyrimidin-7-ium 2,2,2-trifluoroacetate (11b)**

The title compound was prepared by BOC-deprotection of intermediate **11a** according to procedure C to give compound **11b** as a yellow oily liquid (97.6 %). <sup>1</sup>H NMR (300 MHz, DMSO-*d*<sub>6</sub>) δ 9.39 (s, 2H), 8.61 (s, 1H), 7.18 (t,  $J = 8.1$  Hz, 2H), 7.10 (d,  $J = 7.0$  Hz, 1H), 7.00 (t,  $J = 7.2$  Hz, 1H), 4.52 (s, 2H), 3.55 (s, 4H), 3.42 (d,  $J = 4.4$  Hz, 2H), 3.23 (s, 2H), 3.04 (s, 4H), 2.30 (s, 3H). <sup>13</sup>C NMR (75 MHz, DMSO-*d*<sub>6</sub>) δ 167.98, 161.92, 158.27 (q,  $J = 32.5$  Hz), 152.32, 150.88, 131.95, 130.93, 126.58, 126.41, 125.06, 123.29, 119.09, 118.96, 116.94 (q,  $J = 295.3$  Hz), 51.01, 50.62, 46.69, 45.04, 23.35, 17.56. MS (ESI):  $m/z = 366.14$  (M + H)<sup>+</sup>. HRMS (ESI+)  $m/z$  calcd. for C<sub>20</sub>H<sub>24</sub>N<sub>5</sub>S<sup>+</sup> (M + H)<sup>+</sup>: 366.1747 found 366.1742.

**4.5.12. 4-(4-(*m*-tolyl)piperazin-1-yl)-5,6,7,8-tetrahydropyrido[4',3':4,5]thieno[2,3-d]pyrimidin-7-ium 2,2,2-trifluoroacetate (12b)**

The title compound was prepared by BOC-deprotection of intermediate **12a** according to procedure C to give compound **12b** as a white solid (98 %). Melting point 197.6–199 °C. <sup>1</sup>H NMR (300 MHz, DMSO-*d*<sub>6</sub>) δ 9.42 (s, 2H), 8.62 (s, 1H), 7.14 (t,  $J = 7.7$  Hz, 1H), 6.89–6.76 (m, 2H), 6.67 (d,  $J = 7.4$  Hz, 1H), 4.52 (s, 2H), 3.50 (d,  $J = 5.1$  Hz, 4H), 3.41 (d,  $J = 10.8$  Hz, 2H), 3.34 (d,  $J = 4.9$  Hz, 4H), 3.19 (d,  $J = 14.1$  Hz, 2H), 2.27 (s, 3H). <sup>13</sup>C NMR (75 MHz, DMSO-*d*<sub>6</sub>) δ 167.97, 161.98, 158.26 (q,  $J = 35.5$  Hz), 152.36, 150.81, 138.09, 128.83, 126.59, 125.03, 120.37, 119.13, 116.64 (q,  $J = 294.3$  Hz), 116.53, 113.11, 50.11, 48.17, 42.10, 40.81, 23.29, 21.39. MS (ESI):  $m/z = 366.14$  (M + H)<sup>+</sup>. HRMS (ESI+)  $m/z$  calcd. for C<sub>20</sub>H<sub>24</sub>N<sub>5</sub>S<sup>+</sup> (M + H)<sup>+</sup>: 366.1747 found 366.1742.

**4.5.13. 4-(4-(*p*-tolyl)piperazin-1-yl)-5,6,7,8-tetrahydropyrido[4',3':4,5]thieno[2,3-d]pyrimidine, 2,2,2-trifluoroacetate (13b)**

The title compound was prepared by BOC-deprotection of intermediate **13a** according to procedure C to give compound **13b** as a white solid (83.7 %). Melting point 186.8–188.1 °C. <sup>1</sup>H NMR (300 MHz, DMSO-*d*<sub>6</sub>) δ 9.42 (s, 2H), 8.61 (s, 1H), 7.08 (d,  $J = 8.4$  Hz, 2H), 6.94 (d,  $J = 8.6$  Hz, 2H), 4.52 (s, 2H), 3.52 (s, 4H), 3.43 (s, 2H), 3.29 (s, 4H), 3.21 (s, 2H), 2.22 (s, 3H). <sup>13</sup>C NMR (75 MHz, DMSO-*d*<sub>6</sub>) δ 167.97, 161.95,

158.26 (q,  $J = 32.8$  Hz), 152.35, 148.58, 129.45, 128.50, 126.57, 125.03, 119.10, 116.17, 115.84 (q,  $J = 292.2$  Hz), 50.07, 48.61, 42.10, 40.80, 23.28, 20.06. MS (ESI):  $m/z = 366.17$  (M + H)<sup>+</sup>. HRMS (ESI+)  $m/z$  calcd. for C<sub>20</sub>H<sub>24</sub>N<sub>5</sub>S<sup>+</sup> (M + H)<sup>+</sup>: 366.1747 found 366.1742.

**4.5.14. 4-(4-(2-Methoxyphenyl)piperazin-1-yl)-5,6,7,8-tetrahydropyrido[4',3':4,5]thieno[2,3-d]pyrimidin-7-ium 2,2,2-trifluoroacetate (14b)**

The title compound was prepared by BOC-deprotection of intermediate **14a** according to procedure C to give compound **14b** as a white solid (98 %). Melting point 136.6–138.2 °C. <sup>1</sup>H NMR (300 MHz, (CD<sub>3</sub>)<sub>2</sub>CO) δ 8.57 (s, 1H), 7.10–6.97 (m, 3H), 6.96–6.89 (m, 1H), 4.78 (d,  $J = 1.5$  Hz, 2H), 3.87 (s, 3H), 3.76 (t,  $J = 5.8$  Hz, 2H), 3.72–3.62 (m, 4H), 3.54 (t,  $J = 5.8$  Hz, 2H), 3.41–3.28 (m, 4H). <sup>13</sup>C NMR (75 MHz, (CD<sub>3</sub>)<sub>2</sub>CO) δ 169.57, 163.42, 153.53, 153.36, 141.02, 127.25, 126.49, 124.73, 121.94, 120.53, 119.59, 113.19, 55.99, 51.36, 51.18, 43.32, 42.38, 24.49. MS (ESI):  $m/z = 382.18$  (M + H)<sup>+</sup>. HRMS (ESI+)  $m/z$  calcd. for C<sub>20</sub>H<sub>24</sub>N<sub>5</sub>OS<sup>+</sup> (M + H)<sup>+</sup>: 382.1697 found 382.1689.

**4.5.15. 4-(4-(3-Methoxyphenyl)piperazin-1-yl)-5,6,7,8-tetrahydropyrido[4',3':4,5]thieno[2,3-d]pyrimidin-7-ium 2,2,2-trifluoroacetate (15b)**

The title compound was prepared by BOC-deprotection of intermediate **15a** according to procedure C to give compound **15b** as a white solid (95.7 %). Melting point 162.4–164 °C. <sup>1</sup>H NMR (300 MHz, DMSO-*d*<sub>6</sub>) δ 9.42 (s, 2H), 8.62 (s, 1H), 7.15 (t,  $J = 8.2$  Hz, 1H), 6.61 (dd,  $J = 8.3, 1.8$  Hz, 1H), 6.54 (t,  $J = 2.2$  Hz, 1H), 6.43 (dd,  $J = 8.0, 2.0$  Hz, 1H), 4.52 (s, 2H), 3.73 (s, 3H), 3.50 (d,  $J = 4.8$  Hz, 4H), 3.41 (d,  $J = 10.4$  Hz, 2H), 3.35 (s, 4H), 3.21 (s, 2H). <sup>13</sup>C NMR (75 MHz, DMSO-*d*<sub>6</sub>) δ 167.97, 161.95, 160.24, 158.35 (q,  $J = 35.1$  Hz), 152.34, 152.18, 129.70, 126.61, 125.04, 119.12, 116.38 (q,  $J = 293.2$  Hz), 108.40, 104.76, 101.98, 54.93, 50.05, 48.01, 42.08, 40.78, 23.29. MS (ESI):  $m/z = 382.20$  (M + H)<sup>+</sup>. HRMS (ESI+)  $m/z$  calcd. for C<sub>20</sub>H<sub>24</sub>N<sub>5</sub>OS<sup>+</sup> (M + H)<sup>+</sup>: 382.1697 found 382.1691.

**4.5.16. 4-(4-(4-Methoxyphenyl)piperazin-1-yl)-5,6,7,8-tetrahydropyrido[4',3':4,5]thieno[2,3-d]pyrimidin-7-ium 2,2,2-trifluoroacetate (16b)**

The title compound was prepared by BOC-deprotection of intermediate **16a** according to procedure C to give compound **16b** as a white solid (72.2 %). Melting point 178.4–179.6 °C. <sup>1</sup>H NMR (300 MHz, DMSO-*d*<sub>6</sub>) δ 8.54 (s, 1H), 7.01–6.91 (m, 2H), 6.89–6.74 (m, 2H), 4.17 (s, 2H), 3.69 (s, 3H), 3.49 (d,  $J = 5.0$  Hz, 4H), 3.21 (d,  $J = 4.7$  Hz, 4H), 3.06 (d,  $J = 4.6$  Hz, 2H), 3.01 (d,  $J = 4.1$  Hz, 2H). <sup>13</sup>C NMR (75 MHz, DMSO-*d*<sub>6</sub>) δ 167.61, 161.63, 153.22, 151.67, 145.20, 131.90, 126.04, 119.93, 117.77, 114.28, 55.18, 50.15, 49.47, 44.08, 42.11, 26.37. MS (ESI):  $m/z = 382.21$  (M + H)<sup>+</sup>. HRMS (ESI+)  $m/z$  calcd. for C<sub>20</sub>H<sub>24</sub>N<sub>5</sub>OS<sup>+</sup> (M + H)<sup>+</sup>: 382.1697 found 382.1688.

**4.6. Expression and purification of recombinant proteins**

The insert of N-terminally His<sub>6</sub>-tagged human CK2α (sequence with *E. coli*-adapted codons as shown in the Supporting Information) was obtained by commercial gene synthesis from Eurofins Genomics. The insert was sub-cloned in the NdeI/NotI restriction sites of the pET30a vector and transformed into *E. coli* C41(DE3) cells (Sigma-Aldrich, Cat. No. CMC0017). The clone was grown in LB medium containing 50 μg/mL kanamycin and protein expression was induced at an optical density (OD) at 600 nm of 0.8 by the addition of 1.2 mM IPTG. After 3 h, the cell suspension was harvested by centrifugation (30 min, 4000 rpm), the supernatant was discarded, and the resulting pellet frozen at –80 °C. For cell lysis, the cells were thawed on ice and re-suspended in 10 ml of lysis buffer (25 mM Tris HCl pH 8, 150 mM NaCl, 1 mM DTT, 0.5 % Igepal (Sigma-Aldrich, USA) and protease inhibitor cocktail (cComplete Mini, Roche Diagnostics GmbH, Mannheim, Germany). Cell lysis was performed using an ultrasonic disintegrator, with 5 cycles of 20 s each at an amplitude of 80 %. The lysed cell suspension was then centrifuged at 4 °C, 4700 rpm for 40 min. The supernatant was applied to Ni<sup>2+</sup>-NTA agarose beads (QIAGEN GmbH, Hilden, Germany) pre-washed with lysis



buffer. The lysate/bead suspension was mixed overnight on an overhead rotator at 4 °C, then filled in a column with frit, and the beads washed with the following buffers under gravity flow: 4 column volumes of lysis buffer, followed by 4 column volumes of wash buffer (20 mM phosphate buffer pH 7.7, 200 mM NaCl, 20 mM imidazole). The bound protein was then eluted with an elution buffer (20 mM phosphate buffer pH 7.7, 500 mM NaCl, 1 mM DTT, 300 mM imidazole) over 6 column volumes. After elution, the fractions containing protein were pooled and filled in a SERVAPOR® dialysis tube (Cat. No. 44145.01, SERVA Electrophoresis GmbH, Heidelberg, Germany). Dialysis was performed overnight in dialysis buffer A (20 mM phosphate buffer pH 7.7, 500 mM NaCl, 1 mM DTT) to remove the imidazole, and then for 2 h in dialysis buffer B (20 mM phosphate buffer pH 7.7, 500 mM NaCl, 15 % glycerol). The protein was then snap-frozen in liquid nitrogen and stored at -80 °C. Human recombinant CK2 $\alpha_2\beta_2$  was expressed in *E. coli* and purified as previously reported [70,71]. Proteins were quantified using a Bradford assay and the quality of the purification was checked by SDS-PAGE analysis.

#### 4.7. Protein kinase inhibition assays

Kinase Inhibition assays with CK2 $\alpha$  were performed in a reaction buffer containing 50 mM Tris/HCl, pH 7.4, 0.1 mM EGTA, 0.5 mM DTT, 10 mM MgCl<sub>2</sub>, 15  $\mu$ M ATP and 1.0  $\mu$ Ci of [ $\gamma$ -<sup>32</sup>P]-ATP (Hartmann Analytic, Braunschweig, Germany), 280  $\mu$ M of the substrate peptide (sequence H-RRRDDDSDDD-NH<sub>2</sub>, Eurogentech GmbH, Cat. No. AS-60615), and 10 ng of the kinase protein in a final volume of 20  $\mu$ L. The kinase reactions were started by the addition of ATP and performed at 30 °C for 10 min and terminated by spotting 5  $\mu$ L of the reaction mixture onto a nitrocellulose membrane (Amersham™ Protran® Premium, pore size 0.2  $\mu$ m; VWR, Cat. No. 10600014). The membrane was washed four times with 0.3 % phosphoric acid and was left to dry after the final wash. The dry membrane was exposed in a cassette to a Phosphor Screen Imaging Plate (GE Healthcare) and the signals detected by scanning of the imaging plate in a Typhoon FLA 9500 PhosphoImager (GE Healthcare). The spots were quantified using GelQuantNet software to determine the activities of the kinases in the assay reactions. The calculated IC<sub>50</sub> values are representative of at least two independent determinations performed in duplicates.

The kinase inhibition assays with the holoenzyme CK2 $\alpha_2\beta_2$  were performed as previously reported [54]. Briefly, in a final volume of 20  $\mu$ L, CK2 $\alpha$  protein (36 ng) or CK2 $\alpha_2\beta_2$  (40 ng) was incubated in the reaction mixture (20 mM Tris-HCl, pH 7.5, 150 mM NaCl, 1.0 mM DTT) with 1.0 mM of a synthetic substrate peptide, 20 mM MgCl<sub>2</sub>, 1.0  $\mu$ Ci of [ $\gamma$ -<sup>32</sup>P]-ATP and different concentrations of the inhibitor. The final ATP concentration was 10  $\mu$ M if not stated otherwise. The kinase reactions were performed under linear kinetic conditions for 5 min at room temperature, followed by quenching with the addition of 60  $\mu$ L of 4 % TCA. <sup>32</sup>P incorporation in the peptide substrate was determined by spotting the supernatant onto phospho-cellulose paper disks (Whatman P81, 4 cm<sup>2</sup>). The disks were washed three times in cold 0.5 % phosphoric acid, 5 min on a rocking platform per wash, dried and finally the radioactivity was measured. Percentage inhibition was calculated relative to a DMSO control, and all measurements were performed in duplicate. A canonical CK2 peptide substrate (Seq. RRREEDSDDE) phosphorylated equally by CK2 $\alpha_2\beta_2$  and CK2 $\alpha$  (CK2 $\beta$ -independent) was used for the radiometric kinase assays.

The larger panel of kinases shown in Table 4 was screened by the SelectScreen Kinase Profiling Service, Thermo Fisher Scientific, Madison, Wisconsin, USA.

#### 4.8. Cell growth inhibition assay

The 768-O renal carcinoma cell line as well as the U937 histiocytic lymphoma cell line were cultured in RPMI medium with stabilized 2 mM L-glutamine (Sigma-Aldrich) supplemented with 1 % pen/strep solution (Invitrogen) and 10 % fetal calf serum (FCS, Sigma-Aldrich). HEK293

cells were cultured in DMEM medium with stabilized 2 mM L-glutamine (Sigma-Aldrich) supplemented with 1 % pen/strep solution (Invitrogen) and 10 % fetal calf serum (FCS, Sigma-Aldrich). The cells were seeded in a 96 well plate (5000 cells per well) and let to resume growth overnight. The next day, the medium was replaced by medium containing 1 % FCS and either DMSO as a control (max. 0.2 % final concentration) or the test compounds dissolved in DMSO. The cells were grown for 3–4 days at 37 °C in a humidified incubator containing 5 % CO<sub>2</sub>, without further change of medium, before the detection was carried out using 3-(4,5-dimethylthiazol-2-yl)-2,5-diphenyltetrazoliumbromide (MTT, Cat. No. M5655, Sigma-Aldrich) as described previously [72].

#### 4.9. Cell death measurement

786-O cells (3 × 10<sup>3</sup> cells per well) were seeded into 96-well flat-bottom cell culture plates. After 24 h, 10b, CX-4945 or SGC-CK2-1, dissolved in DMSO, were diluted as indicated in the culture medium containing 125 nM Cytotox Green (Sartorius) and added to the cell media, maintaining a final DMSO concentration of 0.2 % (v/v). Experiments were conducted at 37 °C in a 5 % CO<sub>2</sub> atmosphere and the plates were tracked using a CellCyteX live-cell microscopy instrument (Echo). For cell death, Cytotox Green fluorescent cell images were captured every 3 h for the entire duration of the experiment and normalized to the DMSO standard control. The Incucyte Cytotox Green Dye is a fluorescent dye used in cell viability and cytotoxicity assays. The green dye penetrates cells when the integrity of the plasma membrane is compromised and binds to DNA, enabling real-time monitoring of cell death in cell culture experiments.

#### 4.10. Western blot analysis

The test compounds or DMSO as a solvent control were incubated with 786-O cells for 48 h, then the cells were harvested and lysed using Laemmli SDS PAGE buffer. The total protein of the samples was separated by SDS PAGE on precast novex wedgewell™ 8%–16 % gradient gels (Thermo Fischer Scientific, Cat. No. 15486814) at 100 V for 2.5 h. Transfer of the proteins to a 0.45  $\mu$ m immobilon®-FL PVDF membrane (Sigma-Aldrich, Cat. No. IPFL07810) was carried out by semi-dry blotting using a discontinuous buffer system: the blotting paper sheets (BioRad, Cat. No. 170–3965) for the anode were soaked in a buffer containing 60 mM Tris, 40 mM N-cyclohexyl-3-aminopropanesulfonic acid (CAPS), pH 9.6, and 15 % (v/v) methanol in water, and the cathode buffer consisted of 60 mM Tris, 40 mM CAPS, pH 9.6, 15 % (v/v) methanol and 0.1 % SDS in water. Before blotting, the PVDF membrane was prepared by placing it in 100 % methanol, followed by equilibration in anode buffer for 30 min. The protein transfer was carried out for 1 h at 130 mA constant current, after which the membrane was blocked in Rockland blocking buffer for fluorescent western blotting (Biotrend Chemikalien GmbH, Cat. No. MB-070) for 1 h at room temperature. The membrane was then incubated with primary antibodies diluted in Rockland blocking buffer overnight at 4 °C with shaking. Primary antibodies were GAPDH mAb (diluted 1:10000) from ChromoTek GmbH & Proteintech, Germany (Cat. No. 60004-1-Ig), p-STAT3 (Y705) (diluted 1:1000, Cat. No. #9145), CK2 substrate [(pS/pT)DXE] multimer mix (diluted 1:667, Cat. No. #8738), p-cdc37(S13) (D8P8F) mAb (diluted 1:1000, Cat. No. #13248) from Cell Signaling, p-elf2 $\beta$ (Ser2) polyclonal antibody (diluted 1:500, Cat. No. 15504711) from Invitrogen. After washing four times with TBS-T (20 mM Tris-HCl pH 8, 150 mM NaCl, 0.05 % Tween 20) for 15 min each, the membrane was incubated with the secondary antibodies (IR Dye® 680RD goat anti-rabbit, Cat. No. 925–68071, and IR Dye® 800CW goat anti-mouse, Cat. No. 925–32210, from LI-COR, USA, diluted 1:10000 each) for 1 h at room temperature. After washing with TBS-T as above, the fluorescent signals were detected using an ODYSSEY CLx scanner from LI-COR. Images were analyzed using Image Studio software.

#### 4.11. Surface plasmon resonance analysis

SPR binding studies were performed on a Reichert SR7500DC surface plasmon resonance spectrometer (Reichert Technologies, Depew, NY, USA), equipped with medium-density nitrilotriacetic acid (NTA)-derivatized polycarboxylate hydrogel sensor chips NiHC200 M (XanTec Bioanalytics, Düsseldorf, Germany). The chip surface was conditioned by first injecting a 1:1 mixture of 0.5 M EDTA (pH 8.5) and running buffer (10 mM HEPES/NaOH, pH 7.4, 150 mM NaCl, 0.005 % (v/v) Tween-20) for 15 min in both channels at a flow rate of 50  $\mu$ L/min. After a washing step with running buffer for 2 min at a flow rate of 50  $\mu$ L/min, a solution of 5 mM NiCl<sub>2</sub> in running buffer was injected for 2 min at 25  $\mu$ L/min. After another wash step as above, the CK2 $\alpha$  with N-terminal His<sub>6</sub>-tag (40.8 kDa), diluted in 10 mM HEPES, 150 mM NaCl, 0.005 % (v/v) Tween-20, at a final concentration of 6.5  $\mu$ g/mL, was immobilized in one of the two flow cells via affinity-based capturing according to a standard protocol provided by the sensor chip manufacturer. The CK2 $\alpha$  solution was injected at a flow rate of 10  $\mu$ L/min for 7 min. The other flow cell was left blank to serve as a reference. A series of ten buffer injections (running buffer also containing 1 % DMSO (v/v)) was run initially on both reference and active surfaces to equilibrate the system resulting in a stable immobilization level of approximately 3700  $\mu$  refractive index unit ( $\mu$ RIU). Binding and competition experiments were performed at 20 °C. To collect kinetic binding data, analytes with the test compounds dissolved in running buffer with 1 % DMSO (v/v) were injected at a flow rate of 40  $\mu$ L/min for 60 s for monitoring the association followed by the running buffer for 120 s for the dissociation phase. Seven different concentrations were injected, from the lowest concentration to the highest, in both channels. In the competition experiments, a final concentration of 1  $\mu$ M CX-4945 was included in the running buffer with 1 % DMSO (v/v), and binding analysis of the analyte was repeated as before. Differences in the bulk refractive index due to DMSO were corrected by a calibration curve (seven concentrations: 0.25 %, 0.50 %, 0.75 %, 1.0 %, 1.25 %, 1.5 %, and 2.0 % v/v DMSO in running buffer). Data processing and analysis were performed by Scrubber software (Version 2.0c, 2008, BioLogic Software). Sensorgrams were calculated by sequential subtractions of the corresponding curves obtained from the reference flow channel and the running buffer (blank). SPR responses are expressed in resonance unit (RU).

#### 4.12. Molecular modeling

All procedures were performed using the Molecular Operating Environment (MOE) software package (v. 2016, Chemical Computing Group) as described previously [73]. In brief, the docking simulations of **12b** to the 3D coordinates as indicated in the figure legend were performed using the MMFF94x force field; the placement method was set to "triangle" (number of return poses set to 2000), and refinement was set to "induced fit" to enable free side chain movements. After the initial runs, the MOE LigX routine was applied (settings: receptor strength = 5, ligand strength = 5000) for energy minimization, and the best poses selected according to scores. These poses were additionally refined by defining a pharmacophore and re-docking using a pharmacophore-supported placement. The number of retained poses was set to 500 each time. The poses with the top 10 scoring values were further evaluated for plausibility and optimized again using the LigX routine, using the same settings as described above.

#### CRedit authorship contribution statement

**Hend Khalifa:** Writing – original draft, Visualization, Methodology, Investigation. **Ahmed K. ElHady:** Writing – original draft, Methodology, Investigation. **Ting Liu:** Investigation, Formal analysis, Data curation. **Walid A.M. Elgaher:** Supervision, Formal analysis. **Odile Filhol-Cochet:** Investigation. **Claude Cochet:** Investigation. **Ashraf H. Abadi:** Supervision, Conceptualization. **Mostafa M. Hamed:**

Supervision, Methodology. **Mohammad Abdel-Halim:** Writing – review & editing, Supervision, Conceptualization. **Matthias Engel:** Writing – review & editing, Visualization, Supervision, Funding acquisition, Conceptualization.

#### Declaration of competing interest

The authors declare that they have no known competing financial interests or personal relationships that could have appeared to influence the work reported in this paper.

#### Acknowledgment

This work was funded by the Deutsche Forschungsgemeinschaft (DFG, grant No. EN 381/4-1).

#### Appendix A. Supplementary data

Supplementary data to this article can be found online at <https://doi.org/10.1016/j.ejmech.2024.117048>.

#### Data availability

Data will be made available on request.

#### References

- [1] G. Manning, D.B. Whyte, R. Martinez, T. Hunter, S. Sudarsanam, The protein kinase complement of the human genome, *Science* 298 (2002) 1912–1934.
- [2] K. Niefind, B. Guerra, I. Ermakowa, O.G. Issinger, Crystal structure of human protein kinase CK2: insights into basic properties of the CK2 holoenzyme, *EMBO J.* 20 (2001) 5320–5331.
- [3] D.W. Litchfield, Protein kinase CK2: structure, regulation and role in cellular decisions of life and death, *Biochem. J.* 369 (2003) 1–15.
- [4] V. Martel, O. Filhol, A. Nueda, C. Cochet, Dynamic localization/association of protein kinase CK2 subunits in living cells: a role in its cellular regulation? *Ann. N. Y. Acad. Sci.* 973 (2002) 272–277.
- [5] C. Borgo, C. D'Amore, S. Sarno, M. Salvi, M. Ruzzene, Protein kinase CK2: a potential therapeutic target for diverse human diseases, *Signal Transduct. Targeted Ther.* 6 (2021) 183.
- [6] M. Ruzzene, L.A. Pinna, Addiction to protein kinase CK2: a common denominator of diverse cancer cells? *Biochim. Biophys. Acta* 1804 (2010) 499–504.
- [7] J.S. Duncan, J.P. Turowec, G. Vilc, S.S. Li, G.B. Gloor, D.W. Litchfield, Regulation of cell proliferation and survival: convergence of protein kinases and caspases, *Biochim. Biophys. Acta* 1804 (2010) 505–510.
- [8] M.M. Chua, C.E. Ortega, A. Sheikh, M. Lee, H. Abdul-Rassoul, K.L. Hartshorn, I. Dominguez, CK2 in Cancer: Cellular and Biochemical Mechanisms and Potential Therapeutic Target, *Pharmaceuticals* 10 (2017).
- [9] A. Siddiqui-Jain, D. Drygin, N. Streiner, P. Chua, F. Pierre, S.E. O'Brien, J. Bliesath, M. Omori, N. Huser, C. Ho, C. Proffitt, M.K. Schwaeb, D.M. Ryckman, W.G. Rice, K. Anderes, CX-4945, an orally bioavailable selective inhibitor of protein kinase CK2, inhibits prosurvival and angiogenic signaling and exhibits antitumor efficacy, *Cancer Res.* 70 (2010) 10288–10298.
- [10] B. Bestgen, I. Kufareva, W. Seetoh, C. Abell, R.W. Hartmann, R. Abagyan, M. Le Borgne, O. Filhol, C. Cochet, T. Lomberget, M. Engel, 2-Aminothiazole derivatives as selective allosteric modulators of the protein kinase CK2. 2. Structure-based optimization and investigation of effects specific to the allosteric mode of action, *J. Med. Chem.* 62 (2019) 1817–1836.
- [11] M.J. Borad, L.-Y. Bai, M.-H. Chen, J.M. Hubbard, K. Mody, S.Y. Rha, D.A. Richards, S.L. Davis, J. Soong, C.-E.C.-E. Huang, E. Tse, D.H. Ahn, H.-M. Chang, C.-J. Yen, D.-Y. Oh, J.O. Park, C. Hsu, C.R. Becerra, J.-S. Chen, Y.-Y. Chen, Siltmitasertib (CX-4945) in combination with gemcitabine and cisplatin as first-line treatment for patients with locally advanced or metastatic cholangiocarcinoma: a phase Ib/II study, *J. Clin. Oncol.* 39 (2021) 312, 312.
- [12] C.P. Quezada Meza, M. Ruzzene, Protein kinase CK2 and SARS-CoV-2: an expected interplay story, *Kinases Phosphatases* 1 (2023) 141–150.
- [13] H. Kim, K. Choi, H. Kang, S.Y. Lee, S.W. Chi, M.S. Lee, J. Song, D. Im, Y. Choi, S. Cho, Identification of a novel function of CX-4945 as a splicing regulator, *PLoS One* 9 (2014) e94978.
- [14] H. Kim, K.S. Lee, A.K. Kim, M. Choi, K. Choi, M. Kang, S.W. Chi, M.S. Lee, J.S. Lee, S.Y. Lee, W.J. Song, K. Yu, S. Cho, A chemical with proven clinical safety rescues Down-syndrome-related phenotypes through DYRK1A inhibition, *Dis. Model Mech.* 9 (2016) 839–848.
- [15] C. D'Amore, C. Borgo, S. Sarno, M. Salvi, Role of CK2 inhibitor CX-4945 in anti-cancer combination therapy - potential clinical relevance, *Cell. Oncol.* 43 (2020) 1003–1016.

- [16] A.K. ElHady, D.S. El-Gamil, A.H. Abadi, M. Abdel-Halim, M. Engel, An overview of cdc2-like kinase 1 (Cdk1) inhibitors and their therapeutic indications, *Med. Res. Rev.* 43 (2023) 343–398.
- [17] J.T. Rodgers, W. Haas, S.P. Gygi, P. Puigserver, Cdc2-like kinase 2 is an insulin-regulated suppressor of hepatic gluconeogenesis, *Cell Metabol.* 11 (2010) 23–34.
- [18] F. Pierre, S.E. O'Brien, M. Haddach, P. Bourbon, M.K. Schwaeb, E. Stefan, L. Darjania, R. Stansfield, C. Ho, A. Siddiqui-Jain, N. Streiner, W.G. Rice, K. Anderes, D.M. Ryckman, Novel potent pyrimido[4,5-c]quinoline inhibitors of protein kinase CK2: SAR and preliminary assessment of their analgesic and antiviral properties, *Bioorg. Med. Chem. Lett.* 21 (2011) 1687–1691.
- [19] R. Battistutta, G. Cozza, F. Pierre, E. Papinutto, G. Lolli, S. Sarno, S.E. O'Brien, A. Siddiqui-Jain, M. Haddach, K. Anderes, D.M. Ryckman, F. Meggio, L.A. Pinna, Unprecedented selectivity and structural determinants of a new class of protein kinase CK2 inhibitors in clinical trials for the treatment of cancer, *Biochemistry* 50 (2011) 8478–8488.
- [20] Z.W. Davis-Gilbert, A. Kramer, J.E. Dunford, S. Howell, F. Senbabaoglu, C.I. Wells, F.M. Bashore, T.M. Havener, J.L. Smith, M.A. Hossain, U. Oppermann, D. H. Drewry, A.D. Axtman, Discovery of a potent and selective naphthyridine-based chemical probe for casein kinase 2, *ACS Med. Chem. Lett.* 14 (2023) 432–441.
- [21] C.I. Wells, D.H. Drewry, J.E. Pickett, A. Tjaden, A. Kramer, S. Muller, L. Gyenis, D. Menyhart, D.W. Litchfield, S. Knapp, A.D. Axtman, Development of a potent and selective chemical probe for the pleiotropic kinase CK2, *Cell Chem. Biol.* 28 (2021) 546–558, e510.
- [22] M.P. Licciardello, P. Workman, A new chemical probe challenges the broad cancer essentiality of CK2, *Trends Pharmacol. Sci.* 42 (2021) 313–315.
- [23] C. D'Amore, E. Moro, C. Borgo, K. Itami, T. Hirota, L.A. Pinna, M. Salvi, "Janus" efficacy of CX-5011: CK2 inhibition and methuosis induction by independent mechanisms, *Biochim. Biophys. Acta Mol. Cell Res.* 1867 (2020) 118807.
- [24] A. Kramer, C.G. Kurz, B.T. Berger, I.E. Celik, A. Tjaden, F.A. Greco, S. Knapp, T. Hanke, Optimization of pyrazolo[1,5-a]pyrimidines lead to the identification of a highly selective casein kinase 2 inhibitor, *Eur. J. Med. Chem.* 208 (2020) 112770.
- [25] A. Dalle Vedove, F. Zonta, E. Zanforlin, N. Demitri, G. Ribaudo, G. Cazzanelli, A. Ongaro, S. Sarno, G. Zagotto, R. Battistutta, M. Ruzzene, G. Lolli, A novel class of selective CK2 inhibitors targeting its open hinge conformation, *Eur. J. Med. Chem.* 195 (2020) 112267.
- [26] T. Oshima, Y. Niwa, K. Kuwata, A. Srivastava, T. Hyoda, Y. Tsuchiya, M. Kumagai, M. Tsuyuguchi, T. Tamaru, A. Sugiyama, N. Ono, N. Zolboot, Y. Aikawa, S. Oishi, A. Nonami, F. Arai, S. Hagihara, J. Yamaguchi, F. Tama, Y. Kunisaki, K. Yagita, M. Ikeda, T. Kinoshita, S.A. Kay, K. Itami, T. Hirota, Cell-based screen identifies a new potent and highly selective CK2 inhibitor for modulation of circadian rhythms and cancer cell growth, *Sci. Adv.* 5 (2019) eaa9060.
- [27] R. Battistutta, M. Mazzorana, L. Cendron, A. Bortolato, S. Sarno, Z. Kazimierzczuk, G. Zanotti, S. Moro, L.A. Pinna, The ATP-binding site of protein kinase CK2 holds a positive electrostatic area and conserved water molecules, *Chembiochem* 8 (2007) 1804–1809.
- [28] Y. Chen, Y. Wang, J. Wang, Z. Zhou, S. Cao, J. Zhang, Strategies of targeting CK2 in drug discovery: challenges, opportunities, and emerging prospects, *J. Med. Chem.* 66 (2023) 2257–2281.
- [29] K. Chojnacki, P. Winska, M. Wielechowska, E. Lukowska-Chojnacka, C. Tolzer, K. Niefind, M. Bretner, Biological properties and structural study of new aminoalkyl derivatives of benzimidazole and benzotriazole, dual inhibitors of CK2 and PIM1 kinases, *Bioorg. Chem.* 80 (2018) 266–275.
- [30] M.A. Pagano, J. Bain, Z. Kazimierzczuk, S. Sarno, M. Ruzzene, G. Di Maira, M. Elliott, A. Orzeszko, G. Cozza, F. Meggio, L.A. Pinna, The selectivity of inhibitors of protein kinase CK2: an update, *Biochem. J.* 415 (2008) 353–365.
- [31] J. Zhang, P. Tang, L. Zou, J. Zhang, J. Chen, C. Yang, G. He, B. Liu, J. Liu, C. M. Chiang, G. Wang, T. Ye, L. Ouyang, Discovery of novel dual-target inhibitor of bromodomain-containing protein 4/casein kinase 2 inducing apoptosis and autophagy-associated cell death for triple-negative breast cancer therapy, *J. Med. Chem.* 64 (2021) 18025–18053.
- [32] J. Iegre, P. Brear, C. De Fusco, M. Yoshida, S.L. Mitchell, M. Rossmann, L. Carro, H. F. Sore, M. Hyvonen, D.R. Spring, Second-generation CK2alpha inhibitors targeting the alphaD pocket, *Chem. Sci.* 9 (2018) 3041–3049.
- [33] J. Kalia, R.T. Raines, Hydrolytic stability of hydrazones and oximes, *Angew Chem. Int. Ed. Engl.* 47 (2008) 7523–7526.
- [34] F. Qaiser, J.H. Trembley, B.T. Kren, J.J. Wu, A.K. Naveed, K. Ahmed, Protein kinase CK2 inhibition induces cell death via early impact on mitochondrial function, *J. Cell. Biochem.* 115 (2014) 2103–2115.
- [35] J.H. Trembley, B.T. Kren, M. Afzal, G.A. Scaria, M.A. Klein, K. Ahmed, Protein kinase CK2 - diverse roles in cancer cell biology and therapeutic promise, *Mol. Cell. Biochem.* 478 (2023) 899–926.
- [36] A. Bancet, R. Frem, F. Jeanneret, A. Mularoni, P. Bazelle, C. Roelants, J.G. Delcros, J.F. Guichou, C. Pillet, I. Coste, T. Renno, C. Battail, C. Cochet, T. Lomberget, O. Filhol, I. Krimm, Cancer selective cell death induction by a bivalent CK2 inhibitor targeting the ATP site and the allosteric alphaD pocket, *iScience* 27 (2024) 108903.
- [37] G.K. Gray, B.C. McFarland, A.L. Rowse, S.A. Gibson, E.N. Benveniste, Therapeutic CK2 inhibition attenuates diverse pro-survival signaling cascades and decreases cell viability in human breast cancer cells, *Oncotarget* 5 (2014) 6484–6496.
- [38] S. Zanin, C. Borgo, C. Girardi, S.E. O'Brien, Y. Miyata, L.A. Pinna, A. Donella-Deana, M. Ruzzene, Effects of the CK2 inhibitors CX-4945 and CX-5011 on drug-resistant cells, *PLoS One* 7 (2012) e49193.
- [39] C. Franchin, C. Borgo, L. Cesaro, S. Zaramella, J. Vilardell, M. Salvi, G. Arrigoni, L. A. Pinna, Re-evaluation of protein kinase CK2 pleiotropy: new insights provided by a phosphoproteomics analysis of CK2 knockout cells, *Cell. Mol. Life Sci.* 75 (2018) 2011–2026.
- [40] M. Klink, M.A. Rahman, C. Song, P.K. Dhanyamraju, M. Ehudin, Y. Ding, S. Steffens, P. Bhadauria, S. Iyer, C. Aliaga, D. Desai, S. Huang, D. Claxton, A. Sharma, C. Gowda, Mechanistic basis for in vivo therapeutic efficacy of CK2 inhibitor CX-4945 in acute myeloid leukemia, *Cancers* 13 (2021).
- [41] D. Menyhart, L. Gyenis, K. Jurcic, S.E. Roffey, A. Puri, P. Jovanovic, K.J. Szpock, P. Pittock, G. Lajoie, A.D. Axtman, Comparison of CX-4945 and SGC-CK2-1 as inhibitors of CSNK2 using quantitative phosphoproteomics: triple SILAC in combination with inhibitor-resistant CSNK2, *Curr. Res. Chem. Biol.* 3 (2023) 100041.
- [42] F. Llorens, N. Roher, F.A. Miro, S. Sarno, F.X. Ruiz, F. Meggio, M. Plana, L.A. Pinna, E. Itarte, Eukaryotic translation-initiation factor eIF2beta binds to protein kinase CK2: effects on CK2alpha activity, *Biochem. J.* 375 (2003) 623–631.
- [43] L. Gyenis, D. Menyhart, E.S. Cruise, K. Jurcic, S.E. Roffey, D.B. Chai, F. Trifoi, S. R. Fess, P.J. Desormeaux, T. Nunez de Villavicencio Diaz, A.J. Rabalski, S. A. Zukowski, J.P. Turowec, P. Pittock, G. Lajoie, D.W. Litchfield, Chemical genetic validation of CSNK2 substrates using an inhibitor-resistant mutant in combination with triple SILAC quantitative phosphoproteomics, *Front. Mol. Biosci.* 9 (2022) 909711.
- [44] U. Oppermann, D.M. Harris, P. Li, Z. Liu, P. Jain, I. Veletic, A. Ferrajoli, J. Burger, S. O'Brien, P. Bose, P. Thompson, N. Jain, W. Wierda, M.J. Keating, Z. Estrov, Constitutive phosphorylation of STAT3 by the CK2-BLNK-CD5 complex, *Mol. Cancer Res.* 15 (2017) 610–618.
- [45] Y. Zheng, H. Qin, S.J. Frank, L. Deng, D.W. Litchfield, A. Tefferi, A. Pardanani, F. T. Lin, J. Li, B. Sha, E.N. Benveniste, A CK2-dependent mechanism for activation of the JAK-STAT signaling pathway, *Blood* 118 (2011) 156–166.
- [46] H. Hong, E.N. Benveniste, The immune regulatory role of protein kinase CK2 and its implications for treatment of cancer, *Biomedicines* 9 (2021).
- [47] Y. Miyata, E. Nishida, CK2 controls multiple protein kinases by phosphorylating a kinase-targeting molecular chaperone, Cdc37, *Mol. Cell Biol.* 24 (2004) 4065–4074.
- [48] M. Salvi, C. Borgo, L.A. Pinna, M. Ruzzene, Targeting CK2 in cancer: a valuable strategy or a waste of time? *Cell Death Discov.* 7 (2021) 325.
- [49] L. Cesaro, A.M. Zuliani, V. Bosello Travain, M. Salvi, Exploring protein kinase CK2 substrate recognition and the dynamic response of substrate phosphorylation to kinase modulation, *Kinases Phosphatases* 1 (2023) 251–264.
- [50] F. Meggio, L.A. Pinna, One-thousand-and-one substrates of protein kinase CK2? *Faseb. J.* 17 (2003) 349–368.
- [51] B.A. Carneiro, W.S. El-Deiry, Targeting apoptosis in cancer therapy, *Nat. Rev. Clin. Oncol.* 17 (2020) 395–417.
- [52] N. Shahar, S. Larisch, Inhibiting the inhibitors: targeting anti-apoptotic proteins in cancer and therapy resistance, *Drug Resist. Updates* 52 (2020) 100712.
- [53] J. Raaf, E. Brunstein, O.G. Issinger, K. Niefind, The CK2 alpha/CK2 beta interface of human protein kinase CK2 harbors a binding pocket for small molecules, *Chem. Biol.* 15 (2008) 111–117.
- [54] I. Kufareva, B. Bestgen, P. Brear, R. Prudent, B. Laudet, V. Mouchadel, M. Ettaoussi, C.F. Sautel, I. Krimm, M. Engel, O. Filhol, M.L. Borgne, T. Lomberget, C. Cochet, R. Abagyan, Discovery of holoenzyme-disrupting chemicals as substrate-selective CK2 inhibitors, *Sci. Rep.* 9 (2019) 15893.
- [55] S. Wernersson, S. Birgersson, M. Akke, Cosolvent dimethyl sulfoxide influences protein-ligand binding kinetics via solvent viscosity effects: revealing the success rate of complex formation following diffusive protein-ligand encounter, *Biochemistry* 62 (2023) 44–52.
- [56] A. Feoli, G. Sarno, S. Castellano, G. Sbardella, DMSO-related effects on ligand-binding properties of lysine methyltransferases G9a and SETD8, *Chembiochem* 25 (2024) e202300809.
- [57] K. Niefind, O.G. Issinger, Conformational plasticity of the catalytic subunit of protein kinase CK2 and its consequences for regulation and drug design, *Biochim. Biophys. Acta* 1804 (2010) 484–492.
- [58] E. Papinutto, A. Ranchio, G. Lolli, L.A. Pinna, R. Battistutta, Structural and functional analysis of the flexible regions of the catalytic alpha-subunit of protein kinase CK2, *J. Struct. Biol.* 177 (2012) 382–391.
- [59] J. Raaf, K. Klopfleisch, O.G. Issinger, K. Niefind, The catalytic subunit of human protein kinase CK2 structurally deviates from its maize homologue in complex with the nucleotide competitive inhibitor emodin, *J. Mol. Biol.* 377 (2008) 1–8.
- [60] G. Cozza, F. Meggio, S. Moro, The dark side of protein kinase CK2 inhibition, *Curr. Med. Chem.* 18 (2011) 2867–2884.
- [61] O.B. Z, M.F. Moghaddam, A systematic analysis of physicochemical and ADME properties of all small molecule kinase inhibitors approved by US FDA from January 2001 to October 2015, *Curr. Med. Chem.* 24 (2017) 3159–3184.
- [62] M. Montenarh, C. Götz, The interactome of protein kinase CK2, *Protein Kinase CK2*, 2013, pp. 76–116.
- [63] M. Golkowski, A. Lius, T. Sapre, H.-T. Lau, T. Moreno, D.J. Maly, S.-E. Ong, Multiplexed kinase interactome profiling quantifies cellular network activity and plasticity, *Mol. Cell* 83 (2023) 803–818, e808.
- [64] M. Brehme, O. Hantschel, J. Colinge, I. Kaupe, M. Planyavsky, T. Köcher, K. Mechtler, K.L. Bennett, G. Superti-Furga, Charting the molecular network of the drug target Bcr-Abl, *Proc. Natl. Acad. Sci. USA* 106 (2009) 7414–7419.
- [65] C. Olivieri, G.C. Li, Y. Wang, M. Vs, C. Walker, J. Kim, C. Camilloni, A. De Simone, M. Vendruscolo, D.A. Bernlohr, ATP-competitive inhibitors modulate the substrate binding cooperativity of a kinase by altering its conformational entropy, *Sci. Adv.* 8 (2022) eabo0696.
- [66] X. Pan, H. Wang, C. Li, J.Z.H. Zhang, C. Ji, MolGpka: a web server for small molecule pKa prediction using a graph-convolutional neural network, *J. Chem. Inf. Model.* 61 (2021) 3159–3165.
- [67] P.S. Charifson, W.P. Walters, Acidic and basic drugs in medicinal chemistry: a perspective, *J. Med. Chem.* 57 (2014) 9701–9717.

- [68] Z. Rankovic, CNS drug design: balancing physicochemical properties for optimal brain exposure, *J. Med. Chem.* 58 (2015) 2584–2608.
- [69] A.K. ElHady, S.P. Shih, Y.C. Chen, Y.C. Liu, N.S. Ahmed, A.B. Keeton, G.A. Piazza, M. Engel, A.H. Abadi, M. Abdel-Halim, Extending the use of tadalafil scaffold: development of novel selective phosphodiesterase 5 inhibitors and histone deacetylase inhibitors, *Bioorg. Chem.* 98 (2020) 103742.
- [70] D. Leroy, J.K. Heriche, O. Filhol, E.M. Chambaz, C. Cochet, Binding of polyamines to an autonomous domain of the regulatory subunit of protein kinase CK2 induces a conformational change in the holoenzyme. A proposed role for the kinase stimulation, *J. Biol. Chem.* 272 (1997) 20820–20827.
- [71] L. Chantalat, D. Leroy, O. Filhol, A. Nueda, M.J. Benitez, E.M. Chambaz, C. Cochet, O. Dideberg, Crystal structure of the human protein kinase CK2 regulatory subunit reveals its zinc finger-mediated dimerization, *EMBO J.* 18 (1999) 2930–2940.
- [72] M. Mariano, R.W. Hartmann, M. Engel, Systematic diversification of benzylidene heterocycles yields novel inhibitor scaffolds selective for Dyrk1A, Clk1 and CK2, *Eur. J. Med. Chem.* 112 (2016) 209–216.
- [73] A.K. ElHady, M. Abdel-Halim, A.H. Abadi, M. Engel, Development of selective Clk1 and -4 inhibitors for cellular depletion of cancer-relevant proteins, *J. Med. Chem.* 60 (2017) 5377–5391.